Filipa Isabel Peralta da Silva Pereira

Licenciada em Conservação e Restauro

Archaeometallurgical Study of Artefacts From Castro de Vila Nova de São Pedro (Azambuja, Portugal)

Dissertação para obtenção do Grau de Mestre em Conservação e Restauro

Orientador: Rui Jorge Cordeiro Silva, Professor Auxiliar, Faculdade de Ciências e Tecnologia da Universidade Nova de Lisboa
Co-orientadora: Maria de Fátima Duarte Araújo, Investigadora Principal, Instituto Tecnológico e Nuclear
Co-orientador: António Manuel Monge Soares, Investigador Principal, Instituto Tecnológico e Nuclear

Júri:

Presidente: Prof. Doutora Maria João Seixas de Melo
Arguente: Prof. Doutor Francisco Manuel Braz Fernandes
Vogais: Prof. Doutor Rui Jorge Cordeiro Silva,
Prof. Doutora Maria de Fátima Duarte Araújo,
Prof. Doutor António Manuel Monge Soares

FACULDADE DE CIÊNCIAS E TECNOLOGIA
UNIVERSIDADE NOVA DE LISBOA

Outubro de 2011

Estudo arqueometalúrgico de artefactos provenientes do Castro de Vila Nova de São Pedro (Azambuja, Portugal)

Lisboa, 2011

Acknowledgments

This thesis was possible due to the invaluable support and contributions of professors, colleagues, and host institutions (CENIMAT/I3N, ITN and DCR).

I would like to thank my supervisor Professor Rui Jorge Silva and co-supervisors Professor Maria de Fátima Araújo and Professor António Monge Soares for the opportunity to work in a very productive and interesting scientific field. Thanks for all the trust and guidance provided during this last year. For providing archaeological material, the basis of my study, I would like to thank Museu Arqueológico do Carmo.

I also would like to thank all my colleagues Elin Figueiredo, Pedro Valério, Maria João Furtado e Filipa Lopes for having the patience to teach me all about the archaeometallurgical field, always helping me through my questions and doubts.

I acknowledge the financial support from Fundação da Faculdade de Ciências e Tecnologia since this study was initiated in the scope of the research grant from the project METALURGIA PRIMITIVA NO TERRITÓRIO PORTUGUÊS - PTDC/HIS-ARQ/110442/2008.

Finally but not less important, I would like to thank all my friends and family, and specially my partner João Carriço who supported me and helped me through the development and writing of the thesis.

Estudo arqueometalúrgico de artefactos provenientes do Castro de Vila Nova de São Pedro (Azambuja, Portugal)

Filipa Pereira

Resumo

O Castro de Vila Nova de São Pedro (VNSP), localizado no concelho da Azambuja, distrito de Lisboa é um povoado dos III e II Milénios a.C. com uma ocupação predominantemente calcolítica.

Para esta tese foi estudado um conjunto seleccionado de 275 artefactos metálicos (inteiros ou fragmentados) de diferentes tipologias, através de técnicas analíticas não destrutivas ou micro-destrutivas. A classificação dos objectos de acordo com os seus principais elementos químicos foi inicialmente estabelecida por EDXRF. Uma selecção de 53 destes artefactos foi analisada posteriormente por micro-EDXRF para quantificação dos elementos constituintes das ligas. A caracterização microestrutural das ligas, assim como a identificação dos processos termomecânicos aplicados aos artefactos na sua produção, foi efectuada por microscopia óptica apoiada com observações por SEM-EDS e complementada por testes de microdureza Vickers para avaliar a eficácia dos processos termomecânicos na dureza do artefacto.

Os resultados obtidos mostram que a colecção inicial é composta fundamentalmente por cobre ou por cobre arsenical. No subconjunto dos 53 artefactos, 38% consideram-se como uma liga de cobre com arsénio (As>2%) – cobres arsenicais. Foi encontrada uma associação estatística significativa entre o uso de ligas de cobre com conteúdos de arsénio superiores a 2% e os artefactos agrupados por armas. Pode ser indicativo da adição de arsénio na liga de cobre, com vista a aumentar a capacidade mecânica das armas.

A determinação da cadeia operatória pela análise da microestrutura mostra que a maior parte dos artefactos (73%) foram enformados com operações de forja e recozimento e 23% receberam um tratamento de forja a frio final. A presença, em vários casos, de fases ricas em arsénio não evidencia controlo das velocidades de arrefecimento durante os vazamentos. Através dos testes de microdureza Vickers não foi encontrada uma correlação directa entre o conteúdo em arsénio da liga e a sua dureza; mostram no entanto um aumento da dureza nas regiões correspondentes aos gumes dos artefactos.

Palavras chave: Arqueometalurgia, Calcolítico, Cobre, Arsénio.

Archaeometallurgical study of artefacts from Castro de Vila Nova de São Pedro (Azambuja, Portugal)

Filipa Pereira

Abstract

The Castro de Vila Nova de São Pedro (VNSP) is a settlement located at Azambuja, district of Lisbon, occupied during the third and second millennia BC, predominantly during the Chalcolithic period.

A diversified collection of 275 copper-based artefacts (complete or in a fragmented condition) belonging to VNSP was studied for this thesis using non-destructive and micro-destructive analytical techniques. The classification of the objects according to its main chemical elements was performed by using EDXRF spectrometry. A selection of 53 of these artefacts was analysed by micro-EDXRF spectrometry to quantify the alloy compositions. The microstructural characterisation of the metal alloys, as well as the identification of the thermomechanical processes applied to the shaping of the artefacts was accomplished through optical microscopy, supported by SEM-EDS and supplemented by Vickers micro-hardness measures to establish the actual effectiveness of the thermomechanical processes in the hardness of the artefact.

Results show that the initial collection is mainly composed of copper and arsenical copper. In the subset of 53 artefacts, 38% were considered copper alloyed with arsenic (As>2%). A statistically significant association was found between copper alloys with arsenic contents over 2% and artefacts identified as weapons. This could point out as the addition of arsenic in order to increase the weapon's mechanical strength.

The determination of the "chaîne opératoire" by microstructural analysis show that the majority of this subset (73%) was finished with forging plus annealing operations cycles and 23% of the artefacts received final cold hammering. In several cases, the presence of arsenic rich phases in the microstructure shows no evidence of controlling cooling rates during the casting operation. No direct correlation was found between the arsenic content of the alloy and its hardness, assessed by Vickers microhardness testing. Nevertheless, proof was found of a higher hardness near the blade regions of the artefacts.

Keywords: Archaeometallurgy, Chalcolithic, Copper, Arsenic.

Study initiated in the scope of the research grant from the project METALURGIA PRIMITIVA NO TERRITÓRIO PORTUGUÊS - PTDC/HIS-ARQ/110442/2008

Part of this work was selected for oral presentation in IX Congresso Ibérico de Arqueometria, Lisboa, Portugal – 26-28 Outubro de 2011 with the title: “Estudo arqueometalúrgico de artefactos provenientes do Castro de Vila Nova de São Pedro, Portugal” and will be published in the conference proceedings.

An article is also in preparation with the contents of the current thesis.

Index of Contents

Index of Figures

Index of Tables

Symbols and Notations

BA	Bronze Age
BCS	British Chemical Standards
BF	Bright field (in OM observations)
BSE	Backscattered secondary emission (in SEM-EDS analysis)
CA	Copper Age or Chalcolithic Period
CENIMAT	Centro de Investigação de Materiais
DCM	Departamento de Ciências dos Materiais
DCR	Departamento de Conservação e Restauro
DF	Dark field (in OM observations)
EBA	Early Bronze Age
EDXRF	Energy Dispersive X-Ray Fluorescence
FCT	Faculdade de Ciências e Tecnologia
I3N	Instituto de Nanoestruturas, Nanomodelação e Nanofabricação
IA	Iron Age
IGESPAR	Instituto de Gestão do Património Arquitectónico e Arqueológico
IUPAC	International Union of Pure and Applied Chemistry
ITN	Instituto Tecnológico e Nuclear
LBA	Late Bronze Age
MBA	Middle Bronze Age
OM	Optical Microscopy
POL	Cross polarized light (in OM observations)
RH	Relative Humidity
SAM	Studien zu den Anfängen der Mettalurgie (project)
SE	Secondary Electron (in SEM-EDS analysis)
SEM-EDS	Scanning Electron Microscopy – Energy Dispersive Spectroscopy
UNL	Universidade Nova de Lisboa
VHN	Vickers Hardness Number
VNSP	Vila Nova de São Pedro
XRD	X-Ray Diffraction

1. Introduction

Archaeometallurgy allow us to understand the importance of metallurgical activities and its evolution in the social and cultural organization of ancient cultures through the study of metallic artefacts and other remains of metallurgical activities (Craddock, 1995). It is a multidisciplinary approach that involves different areas of knowledge, and allows us to connect the analytical and quantitative results with the archaeological context from which the artefact or artefacts were recovered.

An enormous development occurred during the twentieth century in the field of archaeometallurgy involving the application of analytical techniques, which enable to start large-scale projects (Craddock, 1995), such as the "Studien zu den Anfängen der Metallurgie" (SAM) that produced thousands of analysis of pre- and proto-historic artefacts gathered from all over Europe, including Portugal (Junghans et al., 1968, 1974).

From the late seventies, as a consequence of the installation of non-destructive analytical techniques in Portuguese research centres, the studies concerning chemical composition of pre and proto-historic metallic artefacts and metallurgical debris improved considerably. Many of these studies allowed for an overview of the composition of metals from various Portuguese archaeological contexts. These studies covered a significant chronological period from Chalcolithic (CA) to Iron Age (IA) and were focused mainly on three areas: copper alloys from different pre and proto-historic chronologies (Araújo et al., 2004; Sousa et al., 2004; Valério et al., 2007a,b; Cardoso & Guerra, 1997; Figueiredo et al., 2007, Melo et al., 2009); chemical compositions of pre and proto-historic gold artefacts (Soares et al., 2004, 2010); and the reconsideration of Atlantic and Mediterranean archaeometallurgical influences in Portuguese territory (Cardoso et al., 2002; Melo, 2000).

Lately, research involving some other techniques has provided further significant contributions to the archaeometallurgical field. The microstructural characterization of metal artefacts and metallurgical debris, as well as the relationship between the thermomechanical operational chain used for artefacts prodution and the alloy composition has been recently under investigation in the framework of different research projects. Contributions also have been made relating to social and economic context of metal production. Among them, are worth mentioning the metallic production during Late Bronze Age (LBA) in Central Portugal (Figueiredo et al., 2010; Silva et al., 2008), the identification of very specific manufacturing techniques such as gilding by diffusion at high temperature (Figueiredo et al., 2010), partial melting/solid state diffusion process for the welding of gold button components (Soares et al., 2010) and the establishment of a technological continuity from Late Bronze Age to Early Iron Age bronze metallurgy at the Southwestern Iberian Peninsula (Valério et al., 2010).

Nevertheless, in spite of the considerable progress achieved in recent years, there is still much work to be done concerning the metallurgy found in the Portuguese territory, especially when compared to what has already been done in the remaining area of the Iberian Peninsula (Rovira, 2002). The earlier sites with evidence of metallurgy in the Portuguese territory belong to the transition of the fourth to the third millennium BC (Soares and Cabral, 1993). The study of Chalcolithic materials from Vila Nova de

São Pedro archaeological site is of paramount importance, since a very extensive and diversified metallurgical collection has been recovered at this site, and is deposited at Museu Arqueológico do Carmo (MAC) (Soares, 2005). Their study is of utmost importance on the comprehension of the first steps of the metallurgy not only in the Portuguese Estremadura but also in the Iberian Peninsula.

It is believed that the first metallic elements used during pre-historic times to manufacture artefacts were those present in the native form such as copper, gold or silver. However these last two elements are commonly found associated with each other in their mineral form; frequently native gold is associated with silver forming a natural alloy called electrum. Copper can also be found associated with arsenic (Mohen, 1990).

Later, fortuitous alloys due to the significant presence of other metallic elements in the ores made their appearance. It was through the observation of different characteristics, like higher hardness and/or different colours that led the first metallurgists to experiment the production of copper based alloys. The bronze was certainly the most commonly used alloy during pre-historic times. Bronze alloys were progressively introduced in the Portuguese territory during the Bronze Age (BA ~2250-1200 BC) (Craddock, 1995).

The main subject of study in this thesis is the investigation of coppers and arsenical coppers found in the Portuguese Estremadura, in the Chalcolithic settlement of Vila Nova de São Pedro in order to establish eventual relationships between elemental composition and typology and also to verify eventual correlation between thermomechanical properties, hardness and elemental composition of the artefacts.

1.1 The archaeological site of Vila Nova de São Pedro

The Portuguese Estremadura is a key region in studies of the Chalcolithic period due to the existence of impressive large settlements with evidences of metallurgy (Soares and Cabral, 1993). Three sites: Vila Nova de São Pedro (Azambuja), Zambujal (Torres Vedras) and Leceia (Oeiras) were subject to extensive archaeological excavations, which lead to a comprehensive body of data allowing a reasonable definition of the Chalcolithic culture of the region (Műller et al., 2008). The collection of copper-based materials analysed in this study comes from the settlement of Vila Nova de São Pedro (VNSP) (Figure 1.1).

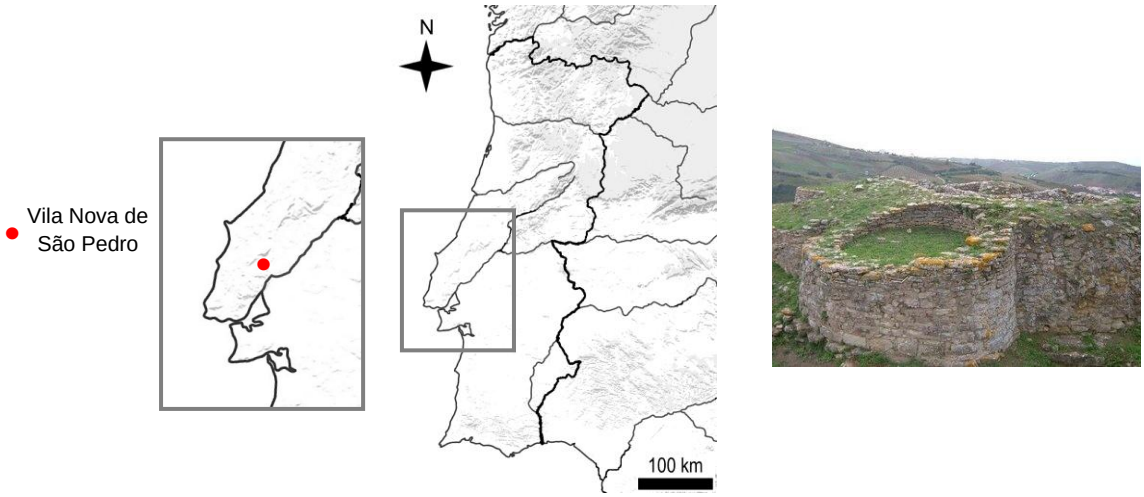

Figure 1.1. Location of the settlement of Vila Nova de São Pedro and some views from the site today.

The Castro de Vila Nova de São Pedro is a Chalcolithic fortified settlement located at Vila Nova de São Pedro (Azambuja, Lisbon). Since 1971, this archaeological site is classified by IGESPAR as a Monument of National Interest.

Its material richness is of great value to the understanding of relevant aspects of pre-historic agricultural societies. The settlement presents a central defensive structure and two outer walls, surrounding the interior where diachronic occupations were found. It was occupied since the Late Neolithic to the Late Chalcolithic or to the Early Bronze Age and may have had sporadic occupations during the Middle Bronze Age. The need to build this complex defensive system is probably due to the accumulation of surplus of agricultural productivity, as inferred from the various excavation campaigns. Alongside agriculture and grazing, some evidence of other practices such as hunting, fishing and gathering were found. Lots of pottery was also collected in the settlement, arrowheads, household utensils, gouges, axes, scrapers and loom weights and articles of worship such as shale, clay and limestone idols. The objects found in VNSP are currently deposited in the Archaeological Museum of Carmo, Lisbon (Soares, 2005) (Figure 1.2).

The defensive structure of this settlement was discovered by Hipólito Raposo in 1936. Following his death, archaeological excavations were carried out in the settlement from 1937 to 1950 by archaeologist Afonso do Paço with the support of Reverend Eugene Jalhay. Unfortunately, there are no field notes of the early excavations. In 1955 and 1959 Edward Sangmeister and Hubert Savory, respectively, participated in the excavations (Műller et al., 2008). Several hundred copper and some bronze artefacts were discovered at VNSP but there are not sufficient studies made of the available materials (Paço, 1952, 1955, 1989; Junghans et al., 1968, 1974). A small part of the metallic collection was analysed in this thesis studies. Despite some general idea about the evolution of the metallurgy in this region (Soares et al., 1996), additional research involving metallic artefacts are needed to answer

more precise and essential questions. These studies could provide important answers about the ancient metallurgy of this region and intercultural relationships with other Iberian prehistoric societies.

Figure 1.2. Exhibition of finds from VNSP at MAC and a model and plan of the archaeological site.

The present work intends to contribute to increase the knowledge of this important Portuguese archaeological site not only by evaluating the arsenic content of copper-based artefacts and correlating it with artefact typologies and functions, but also in the determination of the manufacturing operations involved such as forging and annealing, their evolution and their contribution to the production of harder or stronger metallic material.

2. Experimental Procedure

2.1 Materials

The original collection selected for this study was composed by 275 metallic artefacts or fragments of metallic artefacts, all recovered from Afonso do Paço's archaeological excavations at VNSP. Most of the artefacts could be classified according different typologies: awls, wires, chisels, axes, blades, arrowheads, saws, daggers and a socket. Some of the artefact fragments had an indeterminate typology due to the fact that their size is too small and shapeless to facilitate a correct identification of the object function. An explanation for the shapeless objects and other fragments that show intentional cuts (like de axe's blades) could be that they were scraps or ingots from the manufacturing process and were put aside for posterior remelting. These copper based artefacts were attributed to the Chalcolithic period, but some could already belong to the Early Bronze Age (EBA) due to their typology.

This initial collection of 275 objects was grouped by typologies and each artefact was individually packed and identified. Table 2.1 summarises the division performed and the code assignment: VNSP followed by a number and a letter corresponding to the assigned typology. Images and description of each typology are presented in Appendix I.

Table 2.1. Summary of typologies, quantities and codes attributed.

Typologies*	Number of artefacts	Code (VNSP)
A – Awl	121	001A – 024A; 026A – 122A
B – Wires	9	123B – 131B
C – Chisels	18	132C – 143C; 261C – 266C
D – Axes	43	144D – 176D; 178D; 267D – 275D
E – Blades, Arrowheads	5	179E – 183E
F – Saws	3	185F – 187F
G – Daggers	3	177G; 188G; 189G
H – Socket	1	190H
I – Indeterminate	72	025I; 184I; 191I – 260I
Total	275	

***** In Portuguese: A – Punções; B – Arames; C – Cinzeis; D – Machados; E – Lâminas/Pontas de seta; F – Serras; G – Punhais; H – Alvado; I – Indeterminados

2.2 Methodology

The methodology used in this study consisted of the application of several analytical techniques. These techniques did not require any surface preparation (EDXRF) or involved the removal of the superficial corrosion in a very small area or sampling (micro-EDXRF, OM, SEM-EDS, Vickers micro-hardness testing). Table 2.2 summarises the techniques used to characterize de metallic studied artefacts and main objectives to achieve.

Table 2.2. Techniques used to characterize de metallic artefacts studied in this project.

Analytical Techniques	Number of artefacts analysed	Information expected
EDXRF	Initial group (275 artefacts)	Main alloying elements (corrosion products influence).
Micro-EDXRF	Selection of 53 artefacts	Alloy elemental composition
OM	53	Identification of different phases, inclusions and the thermomechanical processes applied during artefacts production – the operation chain.
SEM-EDS	2	Determination of main chemical phases present in metal alloy and distribution of the chemicals elements and minerals in the inclusions.
Vickers micro-hardness testing	51	Establish the actual effectiveness of the thermomechanical processes in the hardness of the artefact.

The entire collection was first analysed by Energy-Dispersive X-ray Fluorescence Spectrometry (EDXRF), in order to identify the main alloying elements (and some impurities). Subsequently, a subset of 53 artefacts was selected considering several aspects: archaeological significance, typology and conservation condition. From this subset, in 51 cases it was possible to remove a small fragment that was subsequently mounted in epoxy resin and prepared for micro-EDXRF and Optical Microscopy (OM) analysis. One part of the artefact VNSP145D (the cutting edge of an axe) was sampled in two perpendicular cross sections (longitudinal and transversal) and mounted separately in epoxy resin, giving a total number of 54 samples.

The remaining two artefacts had unique characteristics that imposed us a different approach: one of the artefacts (VNSP196I) had a unique circular shape of undetermined typology and the removal of a small sample would interfere with its shape; the other, a saw fragment (VNSP187F) presents a thick corrosion layer and a thin metal core, hence being evaluated too fragile for sampling. Both artefacts were then cleaned from the superficial corrosion layer in a small elliptical area (with approximate 2-3 mm diameter), which was also analysed by micro-EDXRF. The cleaned areas were also observed by OM. The latter procedure was more difficult to perform when compared to samples mounted on resin, and the micrographs often presented imperfections. Nevertheless, this procedure provided a satisfactory interpretation of the microstructure that could be obtained with minimum damage to the artefacts.

Two of the mounted cross-sections were also analysed by Scanning Electron Microscopy with X-ray microanalysis (SEM-EDS).

It is important to keep in mind that the archaeological copper-based artefacts present a characteristic corrosion layer that depends on the conditions of burial. The corrosion products are commonly enriched with some elements, due to the different elemental electrochemical potentials, and due to the different corrosion products stabilities (Robbiola and Portier, 2006). As a result, the elemental composition of archaeological artefacts will usually be different if determined in the surface of the artefact or in a small area cleaned of corrosion products. Therefore the EDXRF was used to identify

the main metal constituents, but these results can only be considered semi-quantitative due to the significant influence of the superficial corrosion layer. Analysing the artefacts by micro-EDXRF spectrometry allow us to determine quantitatively the elemental composition with a minimum damage to the artefact since only a small area of the artefact must be cleaned from the superficial corrosion layer (spot diameter analysed by Micro-EDXRF<100 μm).

The advantages of sampling artefacts for further resin mounting far outweigh the disadvantages in terms of results and possibilities of analysis, if this operation is made carefully and well designed. The removal of samples is performed when the artefact is stable, incomplete and does not affect the visual interpretation. Polished samples mounted in resin are much easier to handle and less dangerous for the artefact when compared to dealing with a localized polished area in the artefact itself. Nevertheless, sometimes the later is the only option available to study an object.

The following sections of the Methodology will detail each analytical technique used.

2.2.1 Energy Dispersive X-ray Spectrometry

A preliminary non-invasive study of 275 fragments of artefacts was conducted in an EDXRF spectrometer (Kevex 771) installed at ITN.

This spectrometer is equipped with a 200 W Rh X-ray tube, secondary excitations targets, radiation filters and a Si(Li) detector with a resolution of 175 eV (Mn-Kα). The characteristic X-rays emitted by chemical elements present in the excited area of the sample (circular shape with a diameter of about 2.5 cm) are measured in a liquid nitrogen cooled Si(Li) detector. The chamber of the spectrometer allows the analysis of whole artefacts with dimensions up to of 35x35x10 cm^3. Details regarding the equipment, analytical conditions and quantifications procedures have been previous published (Kevex, 1992; Araújo et al., 1993).

Each artefact was analysed in one spot, using two excitation conditions – Ag secondary target and Gd secondary target. The analytical conditions used in this study are presented in Table 2.3.

2.2.3. Experimental conditions for EDXRF analyses of copper-based samples.

Excitation	Tube voltage (kV)	Current intensity (mA)	Live time (s)	Elements of interest (with respective X-ray peak)
Ag secondary target	35	0.5	300	Cu-Kα, Pb-Lβ, As-Kα and Fe-Kα Bi-Lα, Zn-Kβ, Ni-Kα
Gd secondary target	57	1.0	300	Sn-Kα Sb-Kα

2.2.2 Micro-Energy Dispersive X-ray Spectrometry

Small cleaned surface areas and mounted cross-sections were analysed with an ArtTAX Pro spectrometer belonging to the DCR.

This micro-EDXRF spectrometer is equipped with a low power 30 W Mo X-ray tube and an electro-thermally cooled silicon drift detector with a resolution of 160 eV (Mn-Kα). Poly capillary lenses collimate the primary X-ray beam enabling a spatial resolution approximately 70-100 μm.

Quantitative analysis was done using WinAxil software (Canberra, 2003) with readings performed in 3 different spots for each artefact. In order to optimize the accuracy of the method, the experimental calibration factors were calculated by the analysis of a standard reference material. This material should have a composition similar to the composition of the samples to be analyzed. For that purpose, a standard material (Phosphor Bronze 551 from British Chemical Standards) was analysed using the same experimental conditions, to calculate the experimental calibration factors for the elements of interest of copper-based alloys. Due to spectral interferences among the As-Kα and Pb-Lα X-ray peaks, the quantification limit for arsenic could not be accurately calculated. The value attributed to arsenic was estimated using the limit of quantification determined for lead due to the similar absorption and enhancement effects in the copper-based matrix. The quantification limits obtained are presented in Table 2.4.

Table 2.4. Quantification limits for EDXRF analyses of copper-based alloys.
(values in %; calculated as 10xbackground$^{0.5}$/sensitivity (IUPAC, 1978) using the standard material Phosphor Bronze 551).

Cu	Sn	Pb	As	Fe	Zn	Ni
0.03	0.60	0.07	0.07	0.05	0.04	0.04

The determination of the accuracy of the analysis made with Micro-EDXRF was accomplished with the quantification of the Phosphor Bronze 552 from British Chemical Standards (Table 2.5).

Table 2.2.5. Accuracy of the micro-EDXRF quantitative analyses of copper-based alloys.
(values in %; * mean value and standard deviation of 3 independent measurements).

Standard	Element	Certified	Obtained*	Relative error (%)
BCS 552	Cu	87.7	88.2 ± 0.6	0.6%
	Sn	9.78	10.1 ± 0.4	0.4%
	Pb	0.63	0.56 ± 0.01	10.4%
	Fe	0.10	0.11 ± 0.02	3.0%
	Ni	0.56	0.51 ± 0.02	15.9%
	Zn	0.35	0.46 ± 0.02	29.0%

The micro-EDXRF exhibits accuracy with low relative errors for the major elements. The minor elements like iron, nickel and zinc present higher relative errors. The zinc and nickel have a strong spectral interference with the alloy main constituent (Cu) and the iron exhibits a spectral interference with escape peak of copper.

2.2.3 Metallographic preparation

Sectioning and Mounting

Samples were extracted from the corresponding archaeological pieces by conventional cutting methods, although applying a special care required for these types of archaeological materials. Due to the small size of the samples, they were fixed in an epoxy resin. Consult Appendix III to see the cross section sampled from each artefact.

Polishing

Mounted cross-sections were polished with SiC abrasive paper (P600, P1000, P2500 and P4000 grit size) and diamond paste (3 μm and 1 μm) using a rotary polishing wheel. Preparation (without sectioning) of small observation areas directly on the artefacts were also manually cleaned and polished with SiC abrasive papers and diamond pastes (6 μm, 3 μm and 1 μm) with the help of a cotton swab. This process removed all cut marks and scratches from the sample surface, allowing for proper material characterization.

Etching

For metallographic observation, etching with a 10% ferrous chloride solution and a time ranging from 3 to 5 s were carried out to reveal microstructural features, like grain boundaries, coring, annealing twins or slip bands.

2.2.4 Optical Microscopy

Metallographic observation of the cross-sections and small superficial areas of cleaned samples were carried out with an optical microscope Leica DMI 5000 M, under bright field (BF), dark field (DF) and polarized light (Pol) illumination. Samples were observed unetched and after etching with an aqueous ferric chloride solution.

2.2.5 Scanning Electron Microscopy with X-ray Microanalysis

Observations on the mounted cross-sections were made in a scanning electron microscope Zeiss DSM 962 equipped with a secondary electrons detector (SE) and a backscattered electrons detector (BSE) installed in CENIMAT.

The equipment also includes an EDS spectrometer Oxford Instruments INCAx-sight with an ultrathin window used for semi-quantitative elemental analysis. For resin mounted samples the metallographic observations were done after the specimen had been sputter coated with carbon.

2.2.6 Vickers MicroHardness Testing

For the subsequent Vickers microhardness studies, mounted cross-sections were again ground and polished to 1μm diamond paste to remove the etched layer. This test was carried out using Zwick-Roell Indentec ZHV μ Micro Hardness testing equipment installed at CENIMAT.

The hardness of a material is defined by its plastic deformation resistance against the penetration by a harder material. The hardness of metals and other no-soft materials is usually given by the Vickers Hardness number (HVN), which is calculated by the load applied over the surface area of the indentation of a diamond pyramid into a prepared surface (Dieter, 1980).

The Vickers micro-hardness was measured in the cleaned areas and avoiding the interference of coarser oxide inclusions or other less representative features. Three indentations were made for each sample with a force of 0.2 Kgf/mm^2 (HV0.2) for 10s. In order to quantify the hardness profiles along a transversal and longitudinal axis, particular procedure was made for artefact VNSP263C: 45 measurements in the longitudinal axis and 15 measurements in the transversal axis.

2.2.7 Statistical Analysis

Statistical analysis was performed using Matlab Version 7.10.0.499 (R2010a) from The Mathworks,Inc (tm). Paired t-tests of the hypothesis that two matched samples come from distributions with equal means were performed using the function “t-test” from the statistics toolbox. Linear regression analysis was performed by the function "polytool” also from the statistics toolbox.

Fisher’s exact test was performed using an online tool available at:
http://www.graphpad.com/quickcalcs/contingency1.cfm

Null hypothesis were rejected at significance levels lower than 5%.

2.2.8 Protection and Chromatic Reintegration of Artefacts

After the analysis and sampling, the artefacts that were prepared for elemental and microstructure characterisation were submitted to a later intervention to avoid the occurrence of corrosion processes in the cleaned or cut area. This conservation treatment consisted essentially in the protection and reintegration of the affected/altered areas. The following steps were applied to all artefacts:

- Application of a corrosion inhibitor Benzotriazol 3% (m/v in ethanol);
- Application of an acrylic resin for protection Paraloid B-72 3% (m/v in ethanol);
- Chromatic reintegration of the area with a mixture of pigments in the Paraloid B-72 media solution to approximate the coloration of the surrounding corrosion products;
- Application of a final protection with a microcrystalline wax dissolved in “*white spirit*”.

The final objective is to return the artefacts to the museum with an individual report consisting of the location of the intervened area and the conservation treatment applied.

3. Results and Discussion

3.1 Alloy type

EDXRF analysis of 275 artefacts was performed to determine the main metal constituents. All the obtained results are presented in Appendix II. A summary is presented in Table 3.1.

The results indicate that the collection of the 275 artefacts is composed mainly by copper (pure copper or copper with some impurities, like arsenic or antimony) and copper with arsenic, where arsenic content seems to be more than vestigial, i.e. an alloy of copper and arsenic (As>2%). Three artefacts revealed to be copper alloyed with tin (bronze) and two to be iron alloys, being then excluded from this study.

Table 3.1. Summary of main elements observed in VNSP artefacts (amount of objects sorted by typologies).

Typologies	Number of artefacts	Cu	Cu+As	Cu+Sn	Fe
A – Awl (punch)	121	93	26	2	0
B – Wires	9	5	4	0	0
C – Chisels	18	5	13	0	0
D – Axes	43	17	26	0	0
E – Blades, Arrowheads	5	0	4	1	0
F – Saws	3	3	0	0	0
G - Daggers	3	0	3	0	0
H – Socket	1	0	1	0	0
I - Indeterminate	72	59	11	0	2
Total	275	182 (66%)	88 (32%)	3 (1%)	2 (1%)

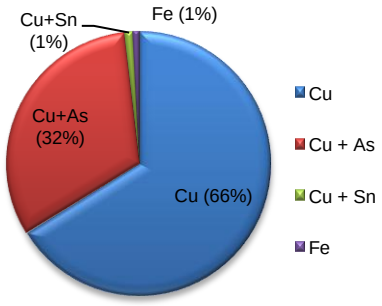

Figure 3.1. Summary of the elemental composition of the 275 VNSP artefacts.

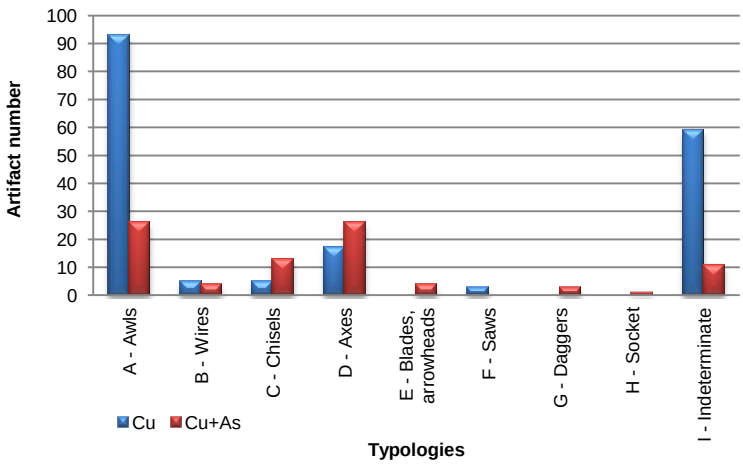

Figure 3.2. Distribution of typologies and composition (Cu and Cu+As).

A summary of the elemental composition of the VNSP artefacts is presented in Figure 3.1 and a distribution of typologies and composition by copper and copper with arsenic is presented in Figure 3.2. Five artifacts composed by Cu+Sn and Fe alloys were excluded because the aim of the study is

the cooper and copper with arsenic artefacts. In this classification of the initial group it is important to refer that no elemental quantification was made for the alloy. Therefore, it is possible that in some of the artefacts considered as made of copper with arsenic, i.e. made of an alloy of these two elements, the arsenic is only present as an impurity (0.07%<As<2%, Northover, 1989) since only the corrosion layers were analysed by EDXRF. It was observed that blades/arrowheads and daggers are all copper with arsenic. Also the number of artefacts of copper with arsenic is higher than the ones only with copper in chisels and axes. In the remaining typologies the higher number of artefacts belongs to the copper group.

Some authors refer that regarding VNSP artefacts collections, weapons systematically contain higher amounts of arsenic than tools. There is also a reference that axes were probably used as ingots and were traded over long distances, and for that reason are not considered weapons (Soares, 2005).

In order to determine if there is an association between the presence and absence of arsenic and the artefact typology (either tools or weapons), three groups of typologies were made: tools (A - awls, C – chisels, D – axes and F - saws), tools excluding axes (A – awls, C – chisels and F – saws) and weapons (E – blades, arrowheads and G - daggers). In the second group it was assumed that axes were used as ingots. For this test we excluded the artifact with a typology of a blade/arrowhead composed by Cu+Sn.

In the analysed collection from VNSP a statistically significant association was found between the fact of being a weapon and the presence of arsenic in the copper alloy (Fisher exact test p=0.0009 when comparing tools including axes and Fisher exact test p=0.0002 when comparing tools excluding axes).

3.2 Alloy composition

As previously explained, a subset of 53 fragments of artefacts was selected to be analysed by micro-EDXRF to establish their elemental composition.

Micro-EDXRF results of metallic artefacts from VNSP are presented in Appendix IV. It indicates that the selected artefacts are composed with copper and copper with arsenic (arsenic contents varying between 0.09% and 9.13%). Furthermore, 21 artefacts exhibit arsenic content that could be considered impurities and not an alloy constituent i.e. 0.07%<As<2% (Northover, 1989). Other 12 exemplars exhibit arsenic content below the detection limit (<0.07%). Ultimately, 20 artefacts, representing 38% of this subset, present arsenic content that could be considered an alloy constituent (As>2%). Iron content is always below the detection limit (<0.05%) with the exception of two artefacts presenting 0.07% and 0.21%.

It was observed that blades/arrowheads presented an arsenic content superior to 2%. On the other hand wires and saws presented an arsenic content below to 1%. In the others typologies there are artefacts with lower and higher arsenic contents with the exception of the socket (As<2%) (Figure 3.3).

Again, a statistically association was found between the fact of being a weapon and the presence of arsenic in the copper alloy (Fisher exact test p=0.0058 when comparing tools including axes and Fisher exact test p=0.0131 when comparing tools excluding axes). Therefore, for this set of weapons it can be hypothesized that there was an intentional addition of arsenic to copper in order to increase its hardness.

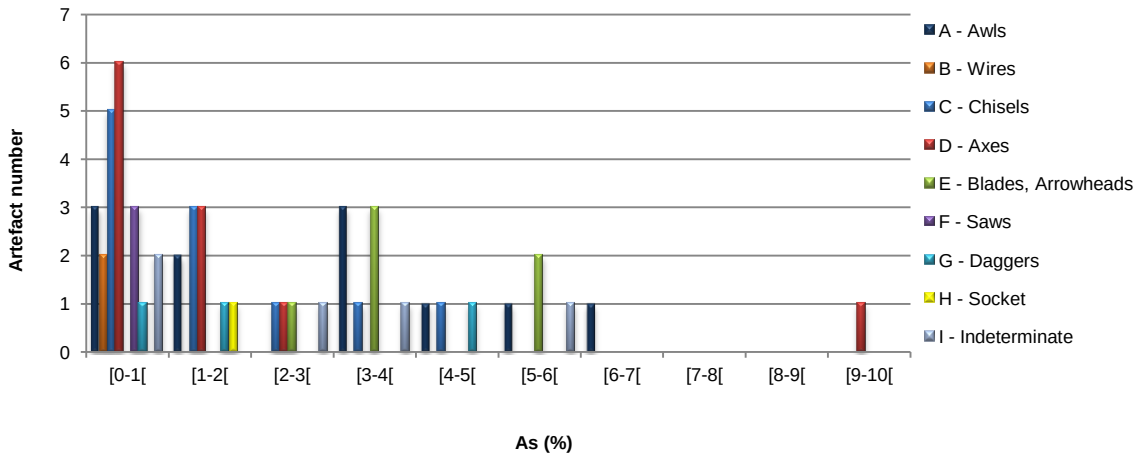

Figure 3.3. Typologies versus As (%) for the 53 artefacts analyzed by micro-EDXRF.

3.3 Microstrutural characterization

OM and SEM-EDS analysis identified different phases, common inclusions and features. Appendix VI provides the summary of the results. The most common manufacturing characteristics were equiaxial grains with annealing twins in the majority of cases and, more rarely, slip bands. Only two cases present as-cast microstructures (C).

In etched samples, annealing twins (recristallization) looks like parallel strips longitudinally enclosed in the α-phase grains. They appear after a metal has been mechanically cold worked (plastically deformed at low temperatures, usually by hammering (F)) and softening by heat treatment (annealing (A)). These cycles (the thermomechanical sequences, hammering plus annealing (F+A)) were established with its characteristic signatures, such as near-equiaxial α-copper grains, having polygonal shapes with straight grain boundaries, annealing twins and elongated inclusions) (Scott, 1991). Slip bands appear in the cold work condition (workhardening) as sets of parallel lines inside the α-phase grains.

Another commonly observed feature is the presence of red inclusions (under DF and Pol ilumination on OM). It was identified by SEM-EDS as being a Cu-O compound, assigned as cuprous oxide (Cu_2O). In other cases the presence of a blue-gray phase was found along the α-copper grain boundaries (under BF, BD and Pol illuminations of OM) and was identified as being a Cu-As rich

phase. A particular case of this arsenic rich phase presenting a heterogeneous morphology was analysed by SEM-EDS and recognized as the copper-arsenide eutectic (α+Cu_3As).

This study established that the majority of the artefacts from VNSP were manufactured with forging and annealing operations (F+A) (Figure 3.4 and 3.5).

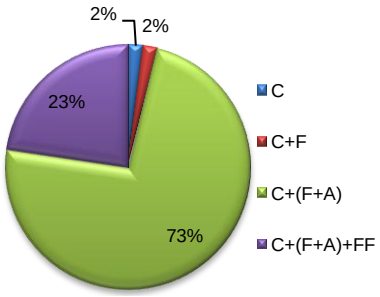

Figure 3.4. Distribution of manufactured procedures in the collection of VNSP studied.

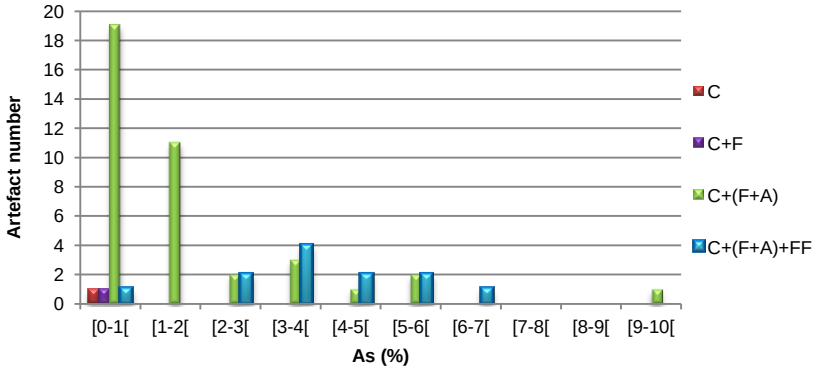

Figure 3.5. Distribution of manufactured procedures versus As (%).

The copper metal solidifies from the liquid state by the nucleation and growth of α-Cu crystals. Usually, with non-pure metals, those crystals grow in preferred directions and form open, tree like structures called dendrites (Figure 3.6). Therefore, as-cast alloy microstructures should present α-Cu dendritic structures. Nevertheless, for slow solidification rates during casting and/or low solute concentrations (such as low alloy elements concentrations and low elemental contaminations) much coarser grain morphology should be expected, sometimes with clear cored grains.

During solidification, oxygen in excess in the liquid metal forms cuprous oxide, originating Cu_2O inclusions. According with thermodynamic equilibrium for the Cu-O system (see binary phase diagram Cu-Cu_2O - Figure 3.7), a lower melting point mixture of α-Cu phase and cuprous oxide, the eutectic (α + Cu_2O) will exist in the as-cast structures. This eutectic appears as an interdendritic network of oxide inclusions in the α-Cu matrix.

The presence in the alloy composition of high oxygen affinity elements, such as As, Sn or P, reduce these cuprous oxide formation. Intense thermomechanical treatments will contribute to destroy the inclusions network.

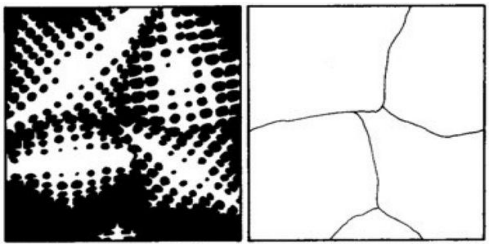

Figure 3.6. As-cast microstructures with columnar dendrites.

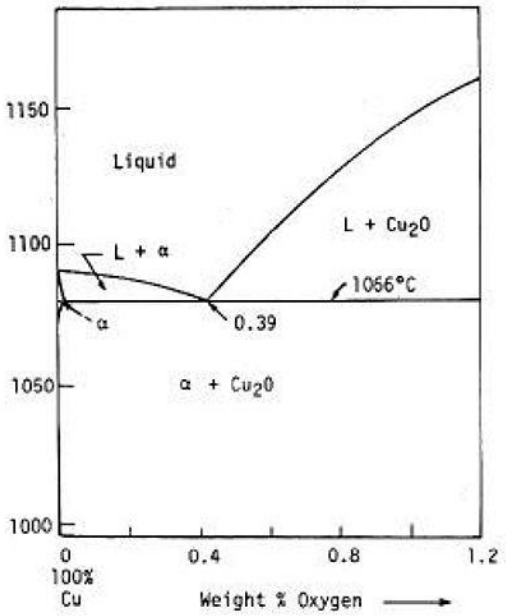

Figure 3.7. Binary diagram Cu-Cu_2O (Cu-O eutectic constituted by α-Cu and Cu_2O) (AMS, 1973).

Only two of the artefacts (of indeterminate typology) analysed present similar characteristics to the as-cast microstructures: VNSP194I e VNSP196I (Figure 3.8). In VNSP194I was possible to observe very large grains (approximately 520 μm) with some deformations which are an indicator of the application of some forging and heating, but not enough to cause a rearrangement (recrystallization) of the grains structure and develop annealing twins.

On the other hand, artefact VNSP196I had dendritic features but since a small area of the surface was cleaned of corrosion products, the columnar dendrites were not clearly visible. The VNSP194I was probably part of an incomplete artefact that was left out before finished and VNSP196I should be a casting droplet taking into account its circular and flatted shape (See Appendix III).

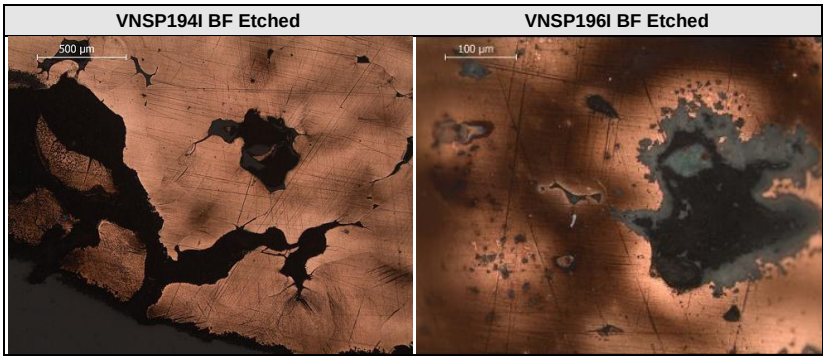

Figure 3.8. MO micrographies of indeterminates VNSP194I and VNSP196I, presenting as-cast microstructures, under BF illumination and after etching.

The artefacts with lower content in arsenic presented cuprous oxide (Cu_2O) inclusions in the characteristic eutectic (α + Cu_2O) islands.

Under BF illumination the Cu_2O are usually dark globular bodies dispersed in a copper background and take a red colour under DF and Pol illumination. Figure 3.9 shows the cuprous oxide particles forming a network, outlining the dendritic grains. This feature was observed in all typologies with low arsenics contents.

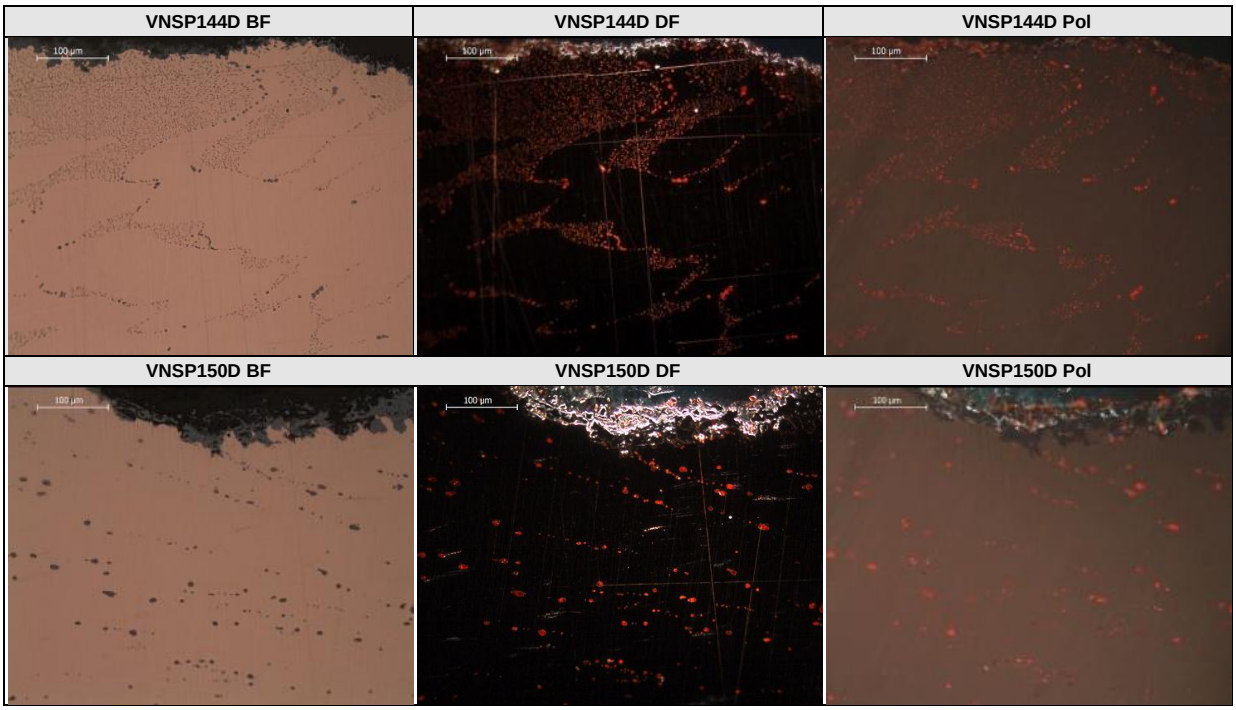

Figure 3.9. MO micrographies of axes VNSP144D (As<0,07%) and VNSP150D (As~0,24%) presenting copper oxides islands in a copper matrix; under BF, DF and Pol illumination.

The interdendritic network of cuprous oxide particles is partial destroyed after thermomechanical operations. Cuprous oxide particles change form, and are present as stringers or aligned rows of dark particles. Due to heating the oxide particles are much larger and fewer in number than in the as-cast microstructure creating what is denominated particle coalescence effect (Scott, 1991).

An example is observed in the axe VNSP178D, where is displayed the rearrangement of these inclusions particles is displayed (Figure 3.10).

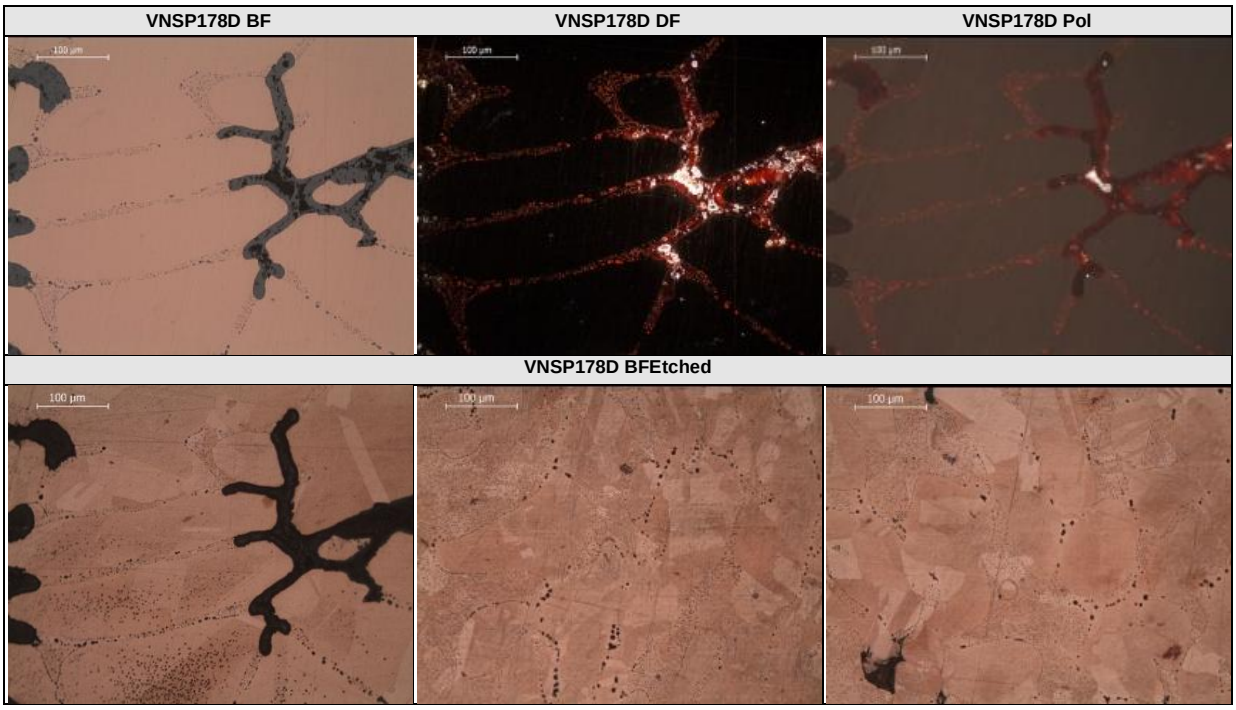

Figure 3.10. MO micrographies of axe VNSP178D revealing the annealing twins and rearrangement of copper oxides, under BF, DF and Pol illumination and after etching.

SEM-EDS analyses were performed at the blade of axe (VNSP268D) to allow a safer confirmation of the oxide nature of the globular phase in the eutectic formation (Figure 3.11). Microanalysis proved that those inclusions are composed by Cu and O.

This axe is an example of an artefact with low content in arsenic (As<0.07%) and presenting the characteristic Cu_2O inclusions in a α-Cu matrix. The cuprous oxide particles form a network, outlining the dendritic cells.

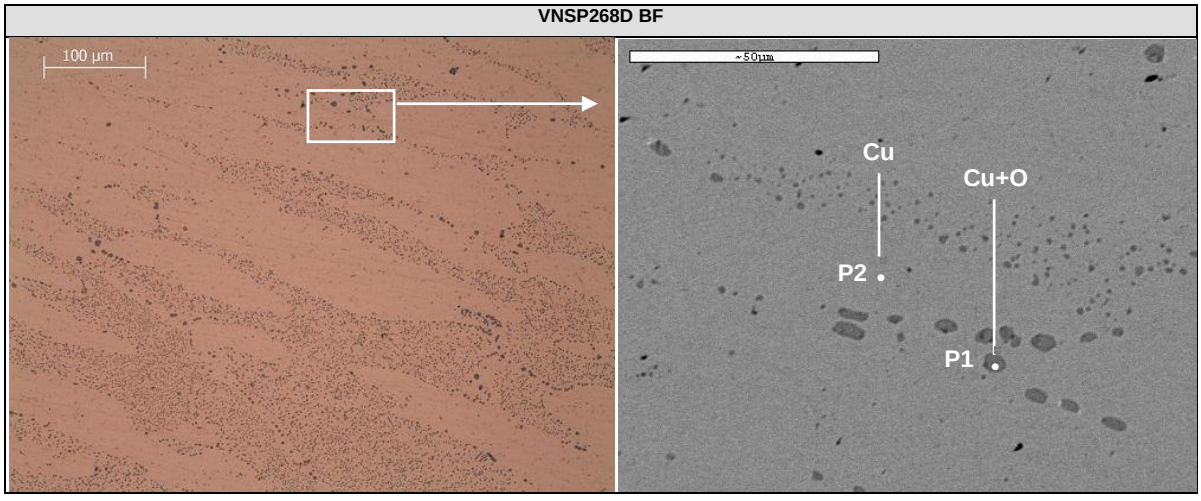

Figure 3.11. MO micrographies of VNSP268D; SEM-BSE image with the region marked on the OM micrography showing the identification of two points by EDS; P1: Cu α phase; P2: Cu_2O inclusions.

The majority of the analysed microstructures display equiaxial grains with annealing twins (Figure 3.12) and some of them also exhibit slip bands (Figure 3.13).

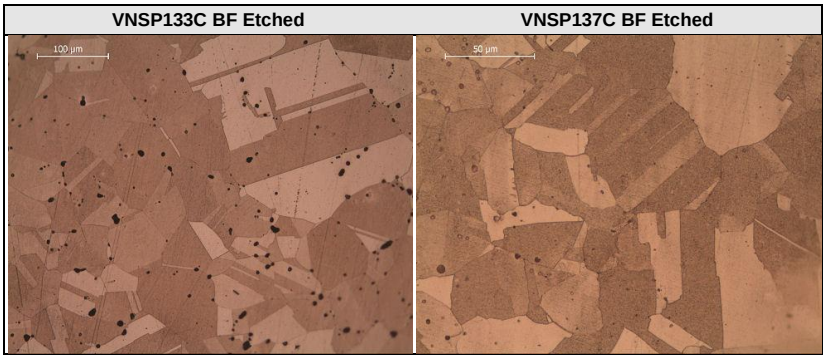

Figure 3.12. MO micrographies of chisels VNSP133C and VNSP137C revealing the annealing twins, under BF illumination and after etching.

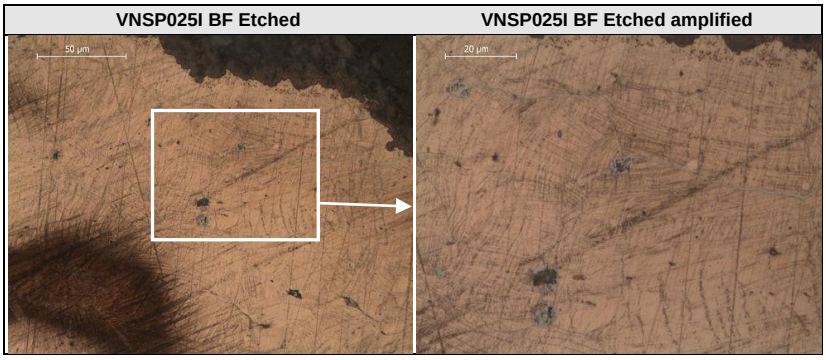

Figure 3.13. MO micrographies of indeterminate VNSP025I revealing slip bands, under BF and after etching.

This indicates the use of one or more cycles of forging plus annealing and also that, in some cases, the operation sequence was finished with forging without subsequent annealing. In most cases, this final forging procedure was not applied, which can be deduced from the absence of slip bands.

Several microstructures exhibited deformed grains and very elongated cuprous oxides, clearly evidencing an important deformation applied to shaping the artefact. In the particular case of artefacts VNSP123B and VNSP124B (both wires) (presented in Figure 3.14), the microstructure that can be observed in the edges show evidence of being cut with some kind of instrument in order to obtain the final width of the artefact.

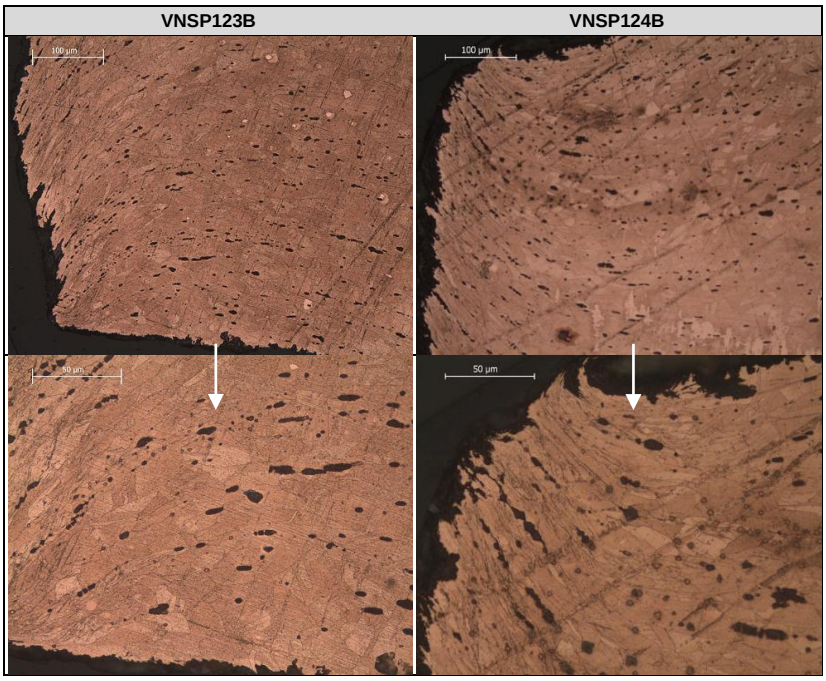

Figure 3.14. MO micrographies of wires VNSP123B and VNSP124B revealing the elongation of the copper oxides by deformation especially in the edges, under BF illumination and after etching.

Due to arsenic segregation during solidification, some artefacts present a primary α-copper phase exhibiting cored grains. Intense mechanical work elongates this features resulting in segregation bands that can be visualized after etching (Figure 3.15).

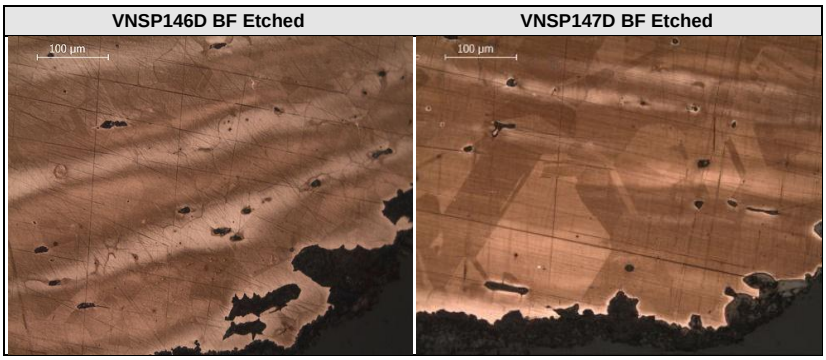

Figure 3.15. MO micrographies of axes VNSP146D and VNSP147D revealing the elongation of the segregation bands, under BF illumination and after etching.

According the Cu-As phase diagram (see Figure 3.17), in equilibrium conditions, the α-Cu phase can dissolve up to approximately 8% of arsenic before the formation of the arsenic rich phase (As-rich (γ) phase – Cu_3As), but under the relatively fast cooling rates of common casting this γ phase has been observed in alloys with only 2% As (Northover, 1989). The fast cooling rate is not unusual because most artefacts have a very small size, but it suggests that there was not any intent to control cooling

process. The thermomechanical procedures of annealing that followed were also not enough to homogenize this kind of alloys.

Therefore, were found artefacts presenting the As-rich (γ) phase (consult Appendix VI) with the characteristics intergranular blue-grey formation in α-copper matrix under BF illumination (under DF and Pol illumination appeared as a darker blue colour) (Figure 3.16). It is also observed a decrease of cuprous oxide, probably due to the deoxidise properties of the arsenic.

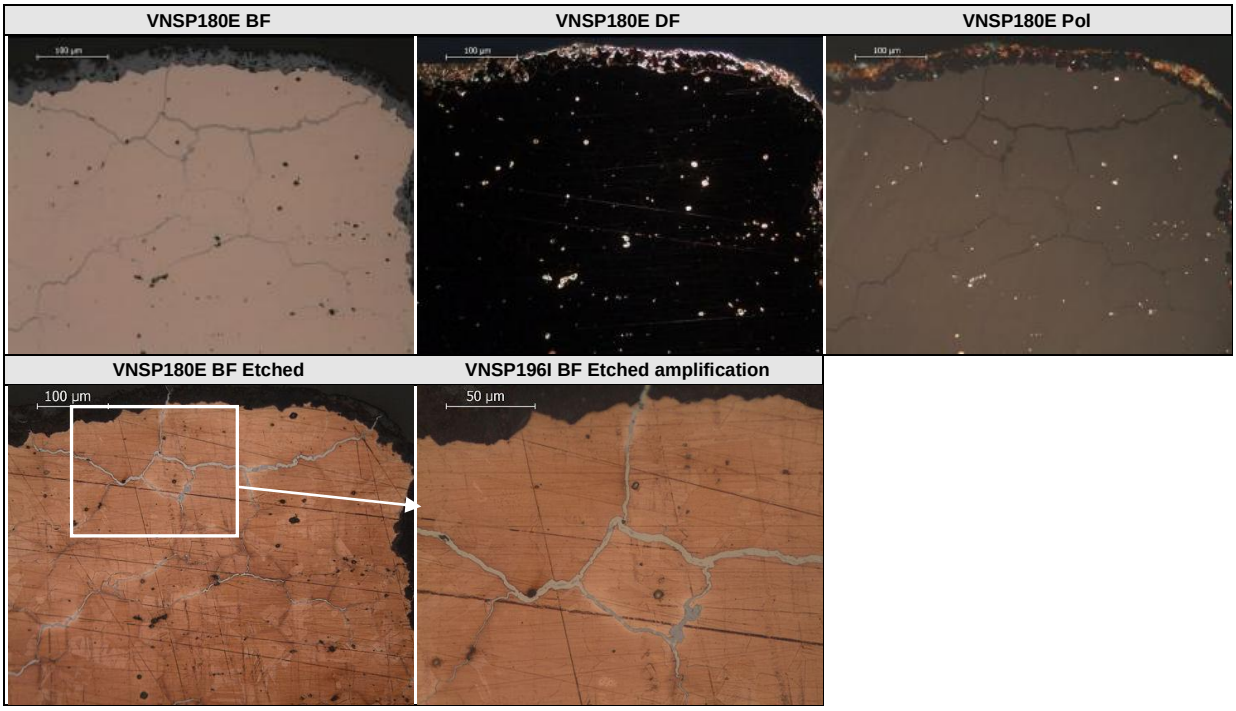

Figure 3.16. MO micrographies of blade VNSP180E revealing the As-rich phase following the grain boundaries, under BF, DF and Pol illumination and after etching.

This As-rich phase (γ) could be the consequence of a phenomenon called inverse segregation. Inverse segregation is a result of shrinkage-driven flow of enriched liquid toward the outer faces (Buschow, K.H.Jürgen et al, 2001), that occurs during casting resulting in a concentration of low melting constituents, as arsenic in copper based alloys, in those regions in which solidification first occurs.

Arsenic segregation in alloys with an overall arsenic content below its solubility limit (7-8% As, in equilibrium) provides evidence of a non-equilibrium solidification after pouring the alloy in the mould.

According to previous studies (Northover, 1989), the annealing of arsenical coppers during ancient times was conducted with temperatures of about 300-400ºC. This range of temperatures is noticeably lower than the temperature necessary (approximately 600-700ºC) to homogenize this type of alloys in a reasonable time. Moreover, the already segregated microstructures could require an even higher temperature to be homogenized (Budd, 1991).

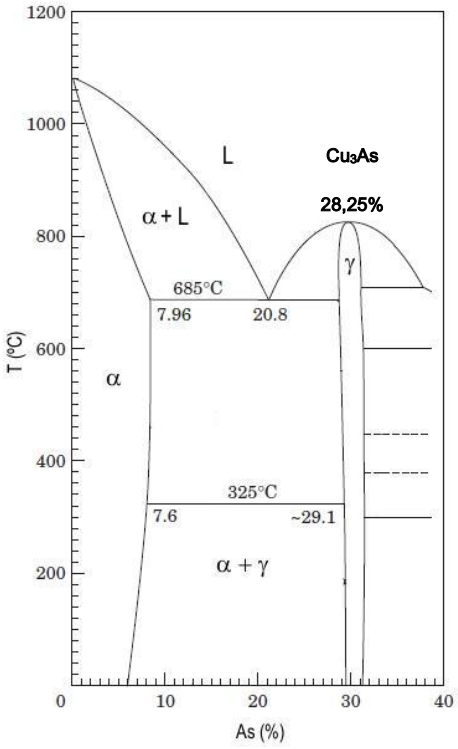

Figure 3.17. Section of Cu-As phase diagram in equilibrium conditions evidencing the formation of the arsenic-rich γ phase at As-richer alloys. (Adapted from Subramanian and Laughlin, 1988).

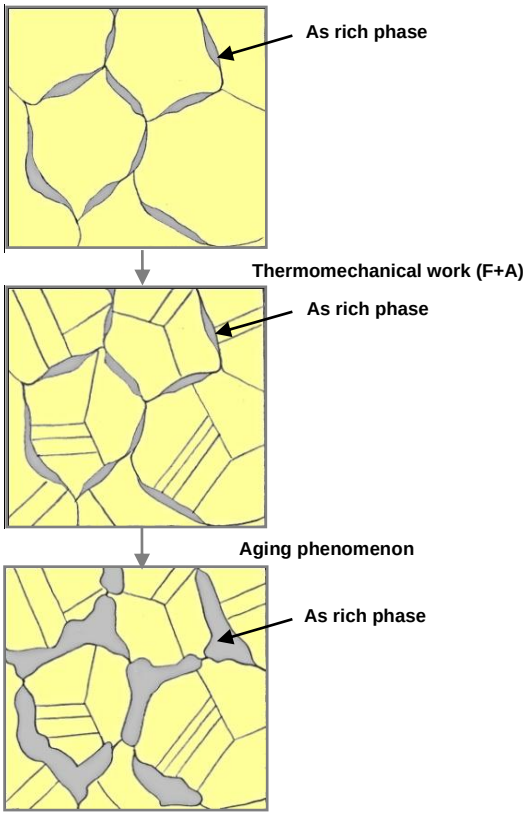

Figure 3.18. Schema representing segregation of arsenic from the solid solution over time, resulting in As-rich phase precipitation – aging process.

It was observed that in some cases the thermomechanical processing (forging plus annealing cycles) in artefacts with arsenic content below its solubility limit is enough to chemically homogenize the alloy, since no arsenic segregations could be observed. Also, the rate of cooling and temperature could be lower enough to minimize the inverse segregation of arsenic. In other cases, the As-rich (γ) phase is still present, mostly in the intergranular α-Cu regions. Examples of this is the awl VNSP001A (As~4.36%) presenting a α-Cu phase and As-rich (γ) and a chisel VNSP140C showing a single phase structure (As~3.43%) (Figure 3.19).

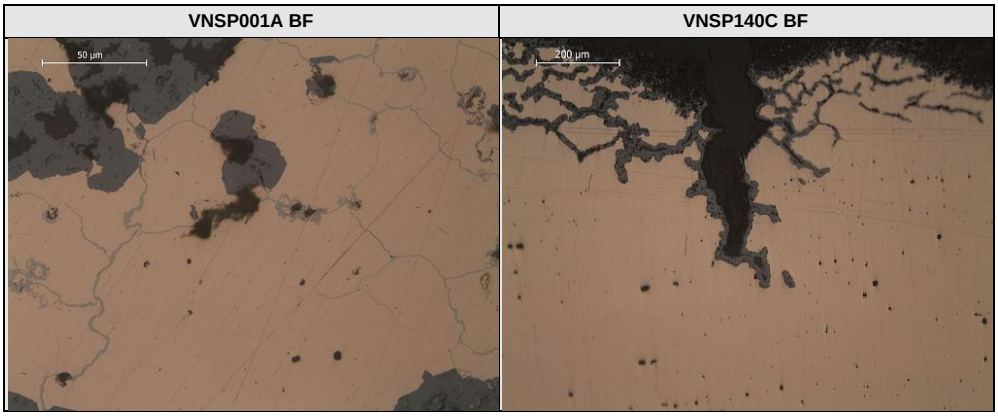

Figure 3.19. MO micrographies of awl VNSP001A and chisel VNSP140C under BF illumination.

The awl is a smaller artefact than a chisel and the control of temperature could be more difficult to accomplish.

Some authors refer that the solubility of arsenic in copper falls markedly at low temperature and that As-rich (γ) phase (Cu_3As) can precipitate from solid solution at ambient temperatures over archaeological times (Budd and Ottaway, 1995). Therefore, the As-rich (γ) phase can precipitate along grain boundaries by natural aging (slow evolution to a more stable condition) during the thousands years in burial context. In those cases the As-rich (γ) phase appears thicker (Schema in Figure 3.18 and examples in Figure 3.20).

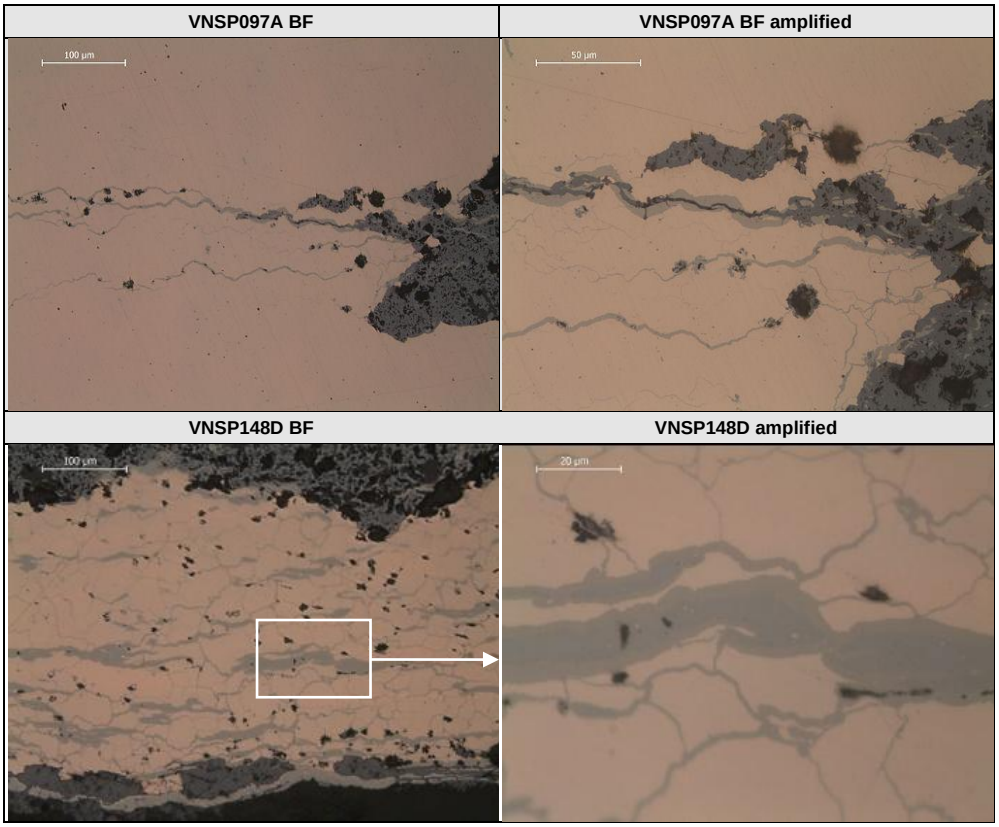

Figure 3.20. MO micrographies of awl VNSP097A and axe VNSP148D revealing a thicker arsenic rich phase following the grain boundaries, under BF illumination.

SEM-EDS microanalyses were performed at the blade of an axe (VNSP148D) to allow a better characterisation of the As-rich (γ) phase developed by inverse segregation. Two different regions of the artefact were studied. According to the equilibrium phase diagram for Cu-As system (Figure 3.17), for hypoeutectic alloys (As<20.8%), the second solidification transformation is the eutectic (α−Cu+γ) formation, where γ (Cu_3As) is constituted by 28.25% As.

In the first region analysed by SEM-EDS (Figure 3.21), the arsenic rich phase seems to form a heterogeneous layer since it shows a small difference in colouration from the centre to the edges. The As-rich (γ) phase presents a composition of 34.3% As in a central a (spot P1) and 32.5% As near the

edge (spot P2). Outside this phase (spot P3) the arsenic content is 6.7%, which is clearly a non-supersaturated α-Cu phase composition.

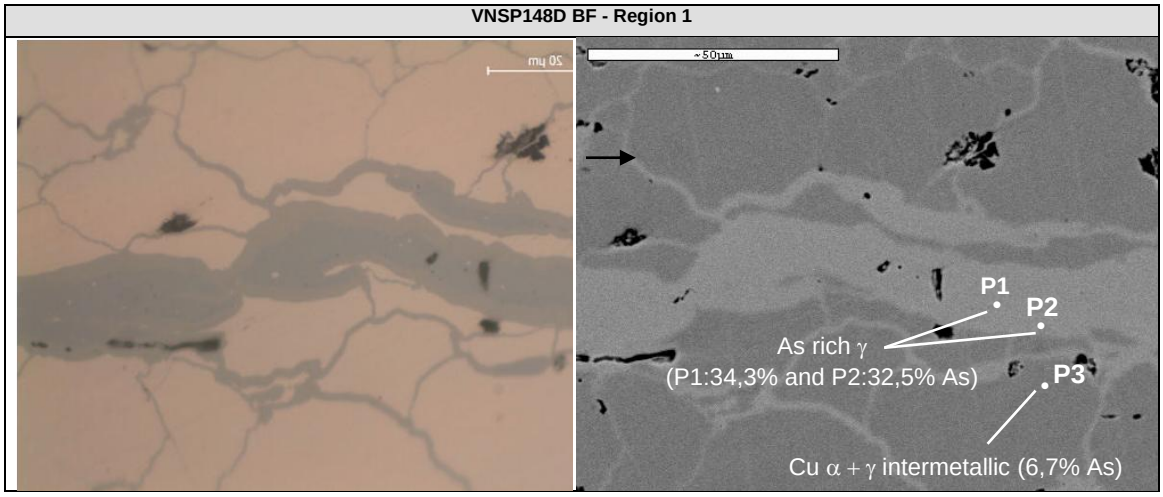

Figure 3.21. MO micrographies analysis of VNSP148D – Region 1; SEM-BSE image with EDS analysis of tree points; P1 and P2: As rich γ phase; P3: Cu α+γ intermetallic phase.

The phenomenon described earlier in Figure 3.18, could explain the compositional gradient observed. Over the years, resulting from an aging process, an increase of arsenic concentration in the As-rich (γ) layer could occur due to precipitation of the γ intermetallic phase from solid solution (Budd and Ottaway, 1995). Also, a preferential copper leaching resulting from corrosion processes would give arsenic concentrations higher than expected.

The second region analysed by SEM-EDS allows the morphologic characterization of the eutectic (α+γ) (Figure 3.22) as being composed by α-Cu islands surrounded by the As-rich (γ) phase. A double layer in the As-rich phase is also observed.

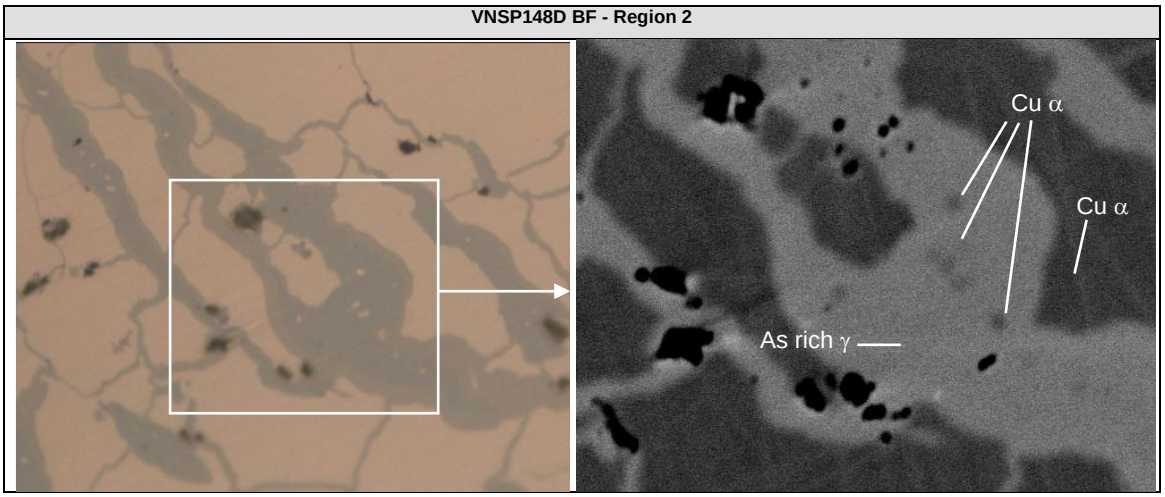

Figure 3.22. MO micrographies of VNSP148D – Region 2; SEM-BSE image with the region marked on the OM micrography showing the determination by EDS of: As rich γ phase; Cu α phase and Cu α islands

3.4 Vickers MicroHardness measurements

In order to study the effect of the mechanical and metallurgical state on the work hardening condition of the outer surface layer, microhardness measurements were made on mounted cross-sections. The microhardness was also determined in the blade area and in the fracture area of the artefacts where a blade exists. The Vickers microhardness measurements (HV0.2) of the 51 artefacts are presented in Appendix V with the exception of the chisel VNSP262C where a transversal and longitudinal microhardness cross-section profiles were obtained and presented separately.

Some authors point to an improvement of the mechanical properties of the resultant metal with the addition of arsenic to copper (Mohen, 1990) plus cycles of forging and annealing. The values of arsenic that are known to enhance the mechanical properties of copper are 3-4% As (Rovira, 2004).
The increased hardness of these alloys could be related to precipitation hardening and higher volume fraction of the As-rich phase. The γ intermetallic precipitates establish strain fields in the matrix and it should lead to an increase in hardness (Budd, 1991).

The results are presented in Figure 3.23, subdivided by operational chain.

In order to determine if there was any correlation between the obtained hardness and arsenic percentage values for the 51 analyzed artefacts, a linear regression was performed and the 95% Confidence Intervals (CI) for the line slope were determined: slope=344.54±354.81. Although the measures show a clear trend toward a positive slope, since the 95% confidence intervals included values less than zero, we cannot exclude the hypothesis of no positive correlation using a linear model. Similar results were obtained when subdividing the analysis by operational sequence, C+F+A or C+F+A+FF.

Therefore, even though it should be expected that the arsenic should confer hardness to the alloy (Mohen, 1990) we did not found any statistically significant association between the arsenic content and the measured hardness. This is probably due to the fact that the material hardness is dependent of other variables, as grain size, phase constitution or degree of work hardening. In certain artefacts hardness measurements could be also affected by deep intragranular corrosion. Consequently, it seems to be difficult to find a clear correlation between the arsenic content and the alloy hardness in these archaeological artefacts. Since studied artefacts presented different typologies, functionalities and diverse corrosion conditions, it was probably necessary a higher or more homogeneous number of samples to obtain a more conclusive result.

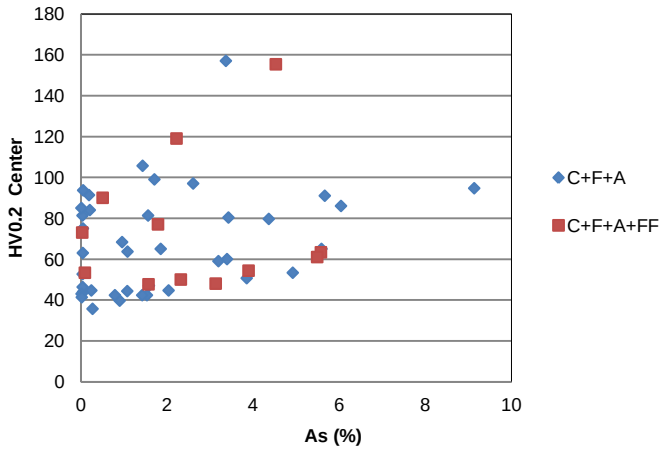

Figure 3.23. Vickers microhardness measurements (HV0.2) versus arsenic content of the artefacts and operational sequence: (C+F) and (C+F)+FF.

In order to compare the hardness in the blade, fracture (opposite side) and central areas for eighteen selected artefacts (Figure 3.24), a paired t-test was performed. The only statistically significant difference at 5% significance level was in the comparison of hardness between the blade and the centre (p=0,037), which reinforces to the conclusion that the blade is harder than the centre. The hardness differences between the fracture and the centre are not statistically significant (p=0.457).

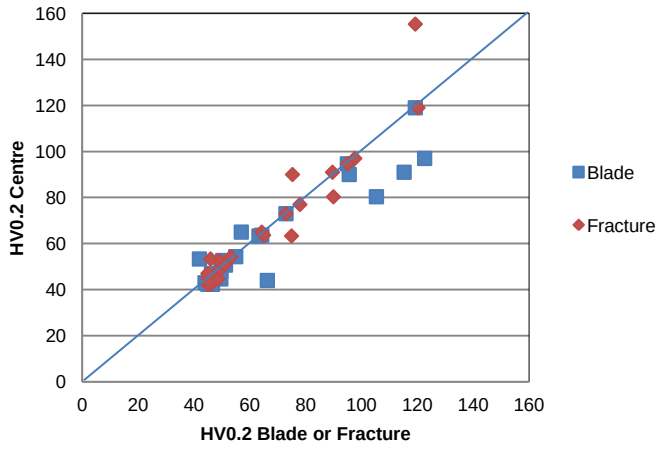

Figure 3.24. Comparison of microhardness measurements (HV0.2) between blade and fracture areas.

The artefact VNSP262C was cut longitudinal and transversal and longitudinal microhardness profiles were measured along the cross section (Figure 3.25). The acquire data is presented in Appendix VII. The measurement data and the profile obtained for each case is presented in Figure 3.26 and Figure 3.27.

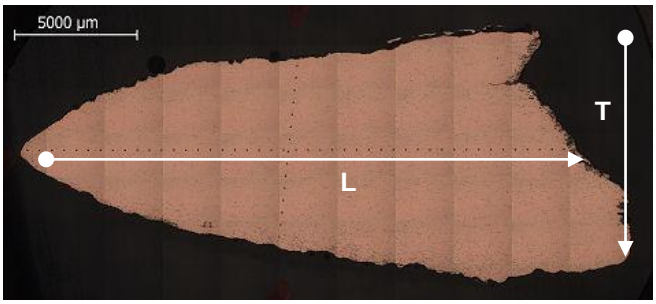

Figure 3.25. View of the orientation of the cut made in the VNSP262C.

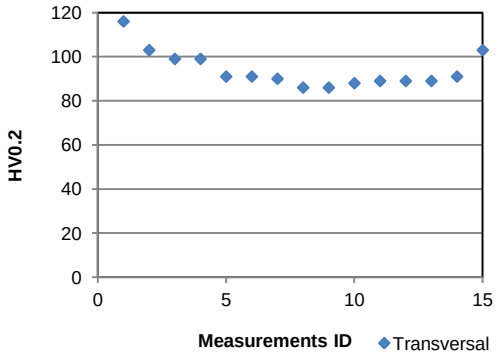

Figure 3.26. Vickers microhardness measurements (HV0.2) in transversal profile of VNSP262C.

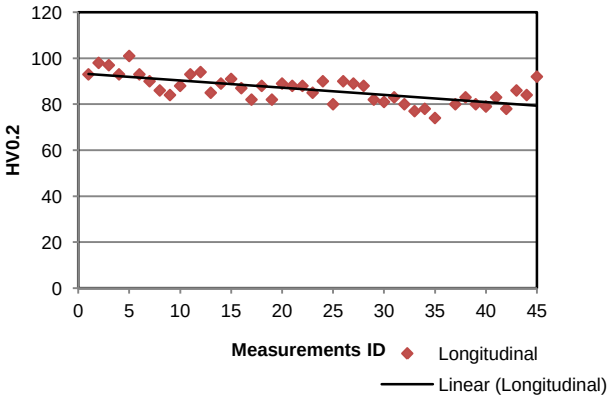

Figure 3.27. Vickers microhardness measurements (HV0.2) in longitudinal profile of VNSP262C.

The chisel VNSP262C is an artefact constituted mainly by copper (As<0.07%) and the "chaîne opératoire" consists in one or more cycles of forging and annealing.

To evaluate if the longitudinal decrease in hardness observed in Figure 3.26 was statistically significant, a linear regression model was evaluated, assuming that all the measurements were evenly spaced. It yielded the following coefficients: slope= -0.322±0.106 for 95% confidence interval and y-axis intercept= 93.637. Since 95% confidence interval for the slope didn't include the value zero, the observed decrease of hardness from the blade to the interior of the artefact was statistically significant at 95% confidence. This means that the thermomechanical work applied in the edge of the chisel imprinted more hardness.

On the other hand the transversal profile seems to indicate increasing close to surfaces (Figure 3.25). However it is not possible to confirm this tendency only with 15 measurements. Larger artefacts should be more adequate to perform microhardness measurements, allowing us to obtain more statistically significant conclusions.

4. Conclusion

This particular collection of the settlement of Vila Nova de São Pedro exhibited great variability of arsenic content, which is in agreement to what is known of the Chalcolithic metallurgical tradition in Portuguese Estremadura (Soares, 2005). This could be explained by the association often found between copper ore and arsenic (Mohen, 1990). It was established in previous studies (Soares et al., 1996) that the copper-based artefacts with significant arsenic contents are common since the middle of the third millennium BC. The introduction of arsenical coppers (As>2%) was understood by some authors as a metallurgical innovation (Craddock, 1995).

Copper artefacts with arsenic contents less than 2% are also among the studied artefacts. The large quantity of artefacts and fragments of artefacts recovered from this site could indicate the existing of recycling operations since the arsenic content decreases with recycling operations.

A statistically significant association was found between copper alloys with arsenic contents over 2% and artefacts identified as weapons. This could point out as the addition of arsenic in order to increase the weapon's mechanical strength.

However, we could hypothesize about the artefacts typology/functionality. Although the majority have been classified as tools, this does not mean that they would be all functional; some could have a ceremonial function or to be a prestige item. Therefore a clear intention of adding arsenic to the alloy to increase hardness could not be established. Functional artefacts would be frequently recycled resulting in reduced arsenic content since each melting of an arsenical copper alloy causes arsenic losses by oxidation and evaporation of As_2O_3 fumes. Other factors, such as the efficient control of the reducing atmosphere during melting and annealing, have as well important consequences in the arsenic content of copper-based artefacts (Mckerrell and Tylecote, 1972).

The high arsenic content of some artefacts could also be associated with their colouring, so artefacts with increased arsenic concentrations present a more yellowish, golden colour that could be considered more suitable for prestige artefacts (Giumlia-Mair, 2005). In the ceremonial artefacts the alloy could have been selected by their colour.

However the operational sequences identified in the manufacture of the artefacts also show that, artefacts with higher arsenic contents, which are harder and more difficult to work, were often mechanically and thermally worked, instead of being kept in as-cast condition. One of the most common operation sequences consisted of one or more cycles of forging and annealing. Annealing restores the ductility lost during hammering, enabling further deformation by forging. These cycles could end with a final forging procedure in order to produce a harder alloy. The operational sequence of annealing of the cast alloy, followed by forging in this group of artefacts is very small. Similar results have been reported in other studies concerning the early metallurgy in the Iberian Peninsula (Rovira, 2004).

The results could indicate a primitive control or a non complete understanding of the purposes of the different metallurgical operations. Inverse segregation of arsenic found in this collection, evidences uncontrolled cooling rates during the casting operation, which difficult any latter thermal homogenisation. This fact could also be explained due to the small size of artefacts since in these cases the cooling velocity is hardly controlled.

The most common manufacturing characteristics identified by OM were equiaxial grains with annealing twins in the majority of cases and, more rarely, slip bands. Another commonly observed feature is the presence of red inclusions (under DF and Pol ilumination). This was identified by SEM-EDS as being the eutectic cuprous oxide (α+Cu_2O). In other cases, the presence of a grey blue phase was found in the intergranular regions (under BF, BD and Pol illuminations of OM) was also identified as being an arsenic rich phase (γ). A particular case of this arsenic rich phase presenting a heterogeneous morphology was tested by SEM-EDS and confirmed to be the eutectic copper arsenide (α+Cu_3As).

Regarding to micro-HV testing, although it should be expected that the arsenic was used to confer hardness to the alloy, it was not found any statistically significant association between the arsenic content and the measured hardness. It should also be expected that an artefact submitted to a final forging step should be harder. However this was not always the case in the artefacts analyzed. It seems that there are many factor to consider together, like intragranular corrosion, grain size, arsenic rich phases, or deformation that influence the hardness of the material. More conclusive results were obtained in a larger artefact (chisel) were a longitudinal measurement line of microhardness was made and a statistically significant decrease of hardness was observed from the edge to the center of the artefact. Larger artefacts would be probably more adequate to perform micro-HV measurements, allowing us to obtain further conclusions.

Since studied artefacts present different typologies, functionalities and corrosion states, it is recommended an investigation of a higher number of samples for each typology in order to achieve more conclusive trends. In the future more studies, including experimental archaeology and archaeometallurgy research, are necessary to better understand the role of arsenic in the copper alloys. For example, one could try to replicate the manufacture procedure of the artefacts. Nevertheless, several difficulties could arise such as the control over As_2O_3 poisoning fumes during these procedures.

The present study allowed some significant considerations regarding the primitive metallurgy at the Portuguese Estremadura territory. The results improved our understanding of the first steps of ancient metallurgy in this region. Future studies of Chalcolithic artefacts and metallurgical remains, including crucibles, slags, and metallic debris from metallurgical operations carried out at VNSP, available on the MAC collection will provide further information on the evolution of the copper-based metallurgy and will contributed to a better knowledge of the overall ancient metallurgy of the Iberian Peninsula.

References

AMS (1973). Metals Handbook 8: Metallography, Structures and Phase Diagrams. Metals Park, OH, American Society for Metals International.

Araújo, M.F., Alves, L.C., Cabral, J.M.P. (1993). Comparison of EDXRF and PIXE in the analysis of ancient gold coins. Nuclear Instruments and Methods in Physics Research B 75(1-4), 450-453.

Araújo, M.F., Barros, L., Teixeira, A.C., Melo, A.A. (2004). EDXRF study of prehistoric artefacts from Quinta do Almaraz (Cacilhas, Portugal). Nuclear Instruments and Methods in Physics Research B 213(1), 741-746.

Budd, P. (1991). Eneolithic arsenical copper: Heat treatment and the metallographic interpretation of manufacturing processes. In: Pernika, E., Wagner, G.A. (Eds.) Proceedings of Archaeometry 90. Basel, Birkhaüser, 35-44.

Budd, P., Ottaway, B.S. (1995). Eneolithic arsenical copper: chance or choice? In: Jovanovic, B. (Ed.) International Symposium Ancient Mining and Metallurgy in Southeast Europe. Archaeological Institute, Donji Milanovac, 95-102.

Canberra (2003). WinAxil Operational Guide. Canberra Eurisys Benelux N.V., Canberra.

Cardoso, J.L., Guerra, M.F. (1997). Análises químicas não destrutivas do espólio metálico do povoado pré-histórico de Leceia, Oeiras e seu significado no quadro da intensificação económica calcolítica da Estremadura portuguesa. Estudos Arqueológicos de Oeiras, 7, 61-67.

Cardoso, J.L. (2000). The fortified site of Leceia (Oeiras) in the context of the Chalcolithic in Portuguese Estremadura. Oxford Journal of Archaeology 19(1), 37-55.

Cardoso, J.L., Soares, A.M.M., Araújo, M.F. (2002). O espólio metálico do Outeiro de S. Bernardo (Moura): uma reapreciação à luz de velhos documentos e de outros achados. O Arqueólogo Português, Série IV, 20, 77-114.

Craddock, P.T. (1995). Early metal mining and production. The University Press, Cambridge.

Dieter, George E. (1980). Mechanical Metallurgy, second edition, International Student Edition, McGraw-Hill International Book Company.

Buschow, K. H. Jürgen et al. (2001). Encyclopedia of Materials: Science and Technology. Elsevier Science Ltd, ISBN: 978-0-08-043152-9, pp. 4733-4739.

Figueiredo, E., Melo, A.Á., Araújo, M.F. (2007). Artefactos metálicos do Castro de Pragança: um estudo preliminar de algumas ligas de cobre por espectrometria de fluorescência de raios X. O Arqueólogo Português 25, 195-215.

Figueiredo E., Silva, R.J.C., Senna-Martinez J.C., Araújo, M.F., Fernandes, F.M.B., VAZ J.L. I. (2010). Smelting and recycling evidences from the Late Bronze Age habitat site of Baiões (Viseu, Portugal). Journal of Archaeological Science, 37, 1623-1634.

Giumlia-Mair, A. (2005). Copper and copper alloys in the Southeastern Alps: an overview. Archaeometry 47(2), 275-292.

IUPAC (1978). Analytical Chemistry Division, Nomenclature, symbols, units and their usage in spectrochemical analysis. Spectrochimica Acta B 33, 242-245.

Junghans, S., Sangmeister, E., Schröder, M. (1968). Kupfer und Bronze in der frühen Metallzeit Europas. Studien zu den Anfängen der Metallurgie 2(1-3), Gebrüder Mann Verlag, Berlin.

Junghans, S., Sangmeister, E., Schröder, M. (1974). Kupfer und Bronze in der frühen Metallzeit Europas. Studien zu den Anfängen der Metallurgie 2(4), Gebrüder Mann Verlag, Berlin.

Kevex (1992). Kevex 771-EDX spectrometer users guide. Kevex Instruments, Valencia.

Lechtman, H., Klein, S. (1999). The production of copper-arsenic alloys (arsenic bronze) by cosmelting: modern experiment, ancient practice. Journal of Archaeological Science 26(5), 497-526.

Mckerrell, H., Tylecote, R.F. (1972). The working of copper-arsenic alloys in the Early Bronze Age and the effect of the determination of provenance. Proceedings of the Prehistoric Society 38, 209–218.

Melo, A.Á. (2000). Armas, utensílios e esconderijos. Alguns aspectos da metalurgia do Bronze Final: o depósito do Casal dos Fiéis de Deus. Revista Portuguesa de Arqueologia 3(1), 15-120.

Melo, A.A., Figueiredo E., Araújo, M.F., Senna-Martinez, J.C. (2009). Fibulae from an Iron Age site in Portugal. Materials and Manufacturing Processes, 24, 955–959.

Mohen, J.P. (1990). Métallurgie préhistorique. Masson, Paris.

Müller, R., Soares, A.M. (2008). Traces of Early Copper Prodution at the Chalcolitic Foritification of Vila Nova de São Pedro (Azambuja, Portugal).

Northover, J.P. (1989). Properties and use of arsenic-copper alloys. In: Hauptmann, A., Pernicka, E., Wagner, G.A. (Eds.) Old World Archaeometallurgy, Deutsches Bergbaumuseum, Bochum, 111-118.

Paço, Afonso do., Arthur, M.L.C. (1952). Castro de Vila Nova de S. Pedro, II – Alguns Objectos Metálicos, in Zephyrus, III, Salamanca, 31-39.

Paço, Afonso do. (1955). Castro de Vila Nova de S. Pedro, VII – Considerações sobre o problema da Metalurgia, in Zephyrus, VI, Salamanca, 27-40.

Paço, Afonso do. (1964). Castro de Vila Nova de S. Pedro, XVI – Metalurgia e Análises Espectrográficas, in Anais da Academia Portuguesa de História, II Série, 14, Lisboa, 159-165.

Robbiola, L., Portier, R. (2006). A global approach to the authentication of ancient bronzes based on the characterisation of the alloy–patina–environment system. Journal of Cultural Heritage 7, 1-12.

Rovira, S. (2002). Metallurgy and society in prehistoric Spain. In: Ottaway, B.S., Wager, E.C. (Eds.) Metals and Society (BAR International Series 1061) Archaeopress, Oxford.

Rovira, S. (2004). Tecnología metalúrgica y cambio cultural en la Prehistoria de la Península Ibérica. Norba. Revista de Historia 17, 9-40.

Scott, David A. (1991). Metallography and Microstructure of Ancient and Historic Metals. The Getty Conservation Institute & Archetype Books.

Silva, R.J.C., Figueiredo, E., Araújo, M.F., Pereira, F. e Fernandes, F.M.B. (2008). Microstructure interpretation of copper and bronze archaeological artefacts from Portugal, Materials Science Forum, 587-588, 365-369.

Soares, A.M.M., Cabral, J.M.P. (1993). Cronologia absoluta para o Calcolítico da Estremadura e do Sul de Portugal. In: 1º Congresso de Arqueologia Peninsular, Actas dos Trabalhos de Antropologia e Etnologia, XXXIII (3-4), Porto, 217-235.

Soares, A.M.M., Araújo, M.F., Alves, L., Ferraz, M.T. (1996). Vestígios metalúrgicos em contextos Calcolíticos e da Idade do Bronze no Sul de Portugal. In: Miscellanea em Homenagem ao Professor Bairrão Oleiro. Edições Colibri, Lisboa, 553-579.

Soares, A.M.M., Valério, P., Araújo, M.F., Alves, L.C. (2004). Análise química não-destrutiva de artefactos em ouro pré e proto-históricos: alguns exemplos. Revista Portuguesa de Arqueologia, 7/2, 125-138.

Soares, A.M.M. (2005). A metalurgia de Vila Nova de São Pedro. Algumas reflexões. In Arnaud, J.M., Fernandes, C. V., eds. – Construindo a memória. As colecções do Museu Arqueológico do Carmo. Lisboa: Associação dos Arqueólogos Portugueses, 179-188.

Soares, A.M.M., Valério, P., Silva, R.J.C., Alves, L.C., Araújo, M.F. (2010). Early Iron Age gold buttons from South-Western Iberian Peninsula. Identification of a gold metallurgical workshop. Trabajos de Prehistoria, 67/2, 501-510.

Sousa, A.C., Valério, P., Araújo, M.F. (2004). Metalurgia antiga do Penedo do Lexim (Mafra). Calcolítico e Idade do Bronze. Revista Portuguesa de Arqueologia 7/2, 97-117.

Subramanian, P.R., Laughlin, D.E. (1988). The As-Cu (Arsenic-Copper) system. Bulletin of Alloy Phase Diagrams 9 (5), 605-617.

Valério, P., Soares, A.M.M., Araújo, M.F., Silva, C.T., Soares, J. (2007a). Vestígios arqueometalúrgicos do povoado calcolítico fortificado do Porto das Carretas (Mourão). O Arqueólogo Português, Série IV, 24, 289-319.

Valério, P., Araújo, M.F., Canha, A. (2007b). EDXRF and Micro-EDXRF studies of Late Bronze Age metallurgical productions from Canedotes (Portugal). Nuclear Instruments and Methods in Physics Research B, 263, 477-482.

Valério, P., Silva, R.J.C,, A.M.M. Soares, M.F. Araújo, F.M. Braz Fernandes, A.C. Silva, L. Berrocal-Rangel (2010). Technological continuity in Early Iron Age bronze metallurgy at the South-Western Iberian Peninsula – a sight from Castro dos Ratinhos. Journal of Archaeological Science, 37, 1811-1919.

Appendix

Appendix I – Photographic documentation of metallic artefacts from VNSP

Figure I.1. Awls: VNSP001A – VNSP0122A.

Figure I.2. Wires: VNSP123B – VNSP131B.

Figure I.3. Chisels: VNSP132C – VNSP143C; VNSP261C – VNSP266C.

a)

b)

c)

Figure I.4. Axes **a)** VNSP144D – VNSP176D; **b)** VNSP267D– VNSP275D; **c)** Distal proximity of Axe VNSP178D.

.

Figure I.5. Blades/arrowheads: VNSP179E – VNSP183E.

Figure I.6. Saws: VNSP185F – VNSP187F.

Figure I.7. Distal proximity of Daggers: VNSP177G; VNSP188G-VNSP189G.

Figure I.8. Socket: VNSP190H.

Figure I.9. Indeterminates: VNSP191I – VNSP259I.

Appendix II – EDXRF experimental results

Table II.1. Summary of the EDXRF experimental results of the fragments of artefacts from VNSP.

Results are semi-quantitative. Legend: n. d.: not detected; +++: Major element; ++ / +: Minor element (Sn, As, Pb); (-): Vestiges; ↓ low amount; ↑ high amount.

Artefact	Semi-quantitative elemental composition (EDXRF)									Obs.
	Cu	Sn	As	Sb	Pb	Fe	Ni	Ca	Elem. (-)	
VNSP001A	+++	n. d.	+	n. d.	n. d.	(-)	n. d.	+	Zn	Cu+As
VNSP002A	+++	n. d.	n. d.	n. d.	n. d.	(-)	n. d.	+	Zn	Cu
VNSP003A	+++	n. d.	+	n. d.	n. d.	+	n. d.	+	Zn	Cu+As
VNSP004A	+++	n. d.	n. d.	n. d.	n. d.	+	(-)	+	Zn	Cu
VNSP005A	+++	n. d.	(-)	n. d.	n. d.	(-)	n. d.	+	Zn	Cu
VNSP006A	+++	n. d.	(-)	n. d.	n. d.	+	(-)	+	Zn	Cu
VNSP007A	+++	n. d.	+	n. d.	n. d.	+	(-)	+	Zn	Cu+As
VNSP008A	+++	n. d.	n. d.	n. d.	n. d.	+	(-)	+	Zn	Cu
VNSP009A	+++	n. d.	+	n. d.	n. d.	+	(-)	+	Zn	Cu+As
VNSP010A	+++	n. d.	+	n. d.	n. d.	+	(-)	+	Zn	Cu+As
VNSP011A	+++	n. d.	n. d.	n. d.	n. d.	+	(-)	+	Zn	Cu
VNSP012A	+++	n. d.	(-)	n. d.	n. d.	+	n. d.	+	Zn	Cu
VNSP013A	+++	n. d.	(-)	n. d.	n. d.	+	n. d.	+	Zn; Bi	Cu
VNSP014A	+++	n. d.	+	n. d.	n. d.	+	(-)	+	Zn; Rb	Cu+As
VNSP015A	+++	n. d.	+	n. d.	n. d.	+	n. d.	+	Zn; Rb	Cu+As
VNSP016A	+++	n. d.	(-)	n. d.	n. d.	+	n. d.	+	Zn	Cu
VNSP017A	+++	n. d.	(-)	n. d.	n. d.	+	n. d.	+	Zn	Cu
VNSP018A	+++	n. d.	+	n. d.	n. d.	+	(-)	+	Zn	Cu+As
VNSP019A	+++	n. d.	n. d.	n. d.	n. d.	+	n. d.	+	Zn	Cu
VNSP020A	+++	n. d.	+	n. d.	n. d.	+	(-)	+	Zn	Cu+As
VNSP021A	+++	n. d.	+	n. d.	n. d.	+	n. d.	+	Zn	Cu+As
VNSP022A	+++	n. d.	+	n. d.	n. d.	+	n. d.	+	Zn	Cu+As
VNSP023A	+++	n. d.	(-)	(-)	n. d.	+	(-)	+	Zn; Bi	Cu
VNSP024A	+++	n. d.	n. d.	n. d.	n. d.	+	(-)	+	Zn	Cu
VNSP026A	+++	n. d.	n. d.	n. d.	n. d.	+	(-)	+	Zn	Cu
VNSP027A	+++	n. d.	n. d.	n. d.	n. d.	+	(-)	(-)	Zn	Cu
VNSP028A	+++	n. d.	n. d.	n. d.	n. d.	+	(-)	(-)	Zn	Cu
VNSP029A	+++	n. d.	+	n. d.	n. d.	+	(-)	+	Zn	Cu+As
VNSP030A	+++	n. d.	n. d.	n. d	n. d.	+	(-)	+	Zn	Cu
VNSP031A	+++	n. d.	+	n. d.	n. d.	+	(-)	+	Zn	Cu+As
VNSP032A	+++	n. d.	(-)	n. d.	n. d.	+	(-)	+	Zn	Cu
VNSP033A	+++	n. d.	(-)	n. d.	n. d.	+	(-)	+	Zn	Cu
VNSP034A	+++	n. d.	n. d.	n. d.	n. d.	+	(-)	+	Zn	Cu
VNSP035A	+++	n. d.	+	n. d.	n. d.	+	(-)	+	Zn	Cu+As
VNSP036A	+++	n. d.	(-)	n. d.	n. d.	+	(-)	+	Zn	Cu
VNSP037A	+++	n. d.	(-)	n. d.	n. d.	+	(-)	+	Zn	Cu
VNSP038A	+++	n. d.	(-)	n. d.	n. d.	+	(-)	+	Zn	Cu
VNSP039A	+++	n. d.	(-)	n. d.	n. d.	+	(-)	+	Zn	Cu
VNSP040A	+++	n. d.	(-)	n. d.	n. d.	+	(-)	+	Zn	Cu
VNSP041A	+++	n. d.	+	n. d.	n. d.	+	(-)	(-)	Zn	Cu+As
VNSP042A	+++	n. d.	(-)	n. d.	n. d.	+	n. d.	(-)	Zn	Cu
VNSP043A	+++	n. d.	n. d.	n. d.	n. d.	+	n. d.	+	Zn	Cu
VNSP044A	+++	n. d.	(-)	n. d.	n. d.	+	(-)	+	Zn	Cu
VNSP045A	+++	n. d.	n. d.	n. d.	n. d.	+	(-)	+	Zn	Cu
VNSP046A	+++	n. d.	n. d.	n. d.	n. d.	+	n. d.	+	Zn	Cu
VNSP047A	+++	n. d.	n. d.	n. d.	n. d.	+	n. d.	+	Zn	Cu
VNSP048A	+++	n. d.	(-)	n. d.	n. d.	+	(-)	n. d.	Zn	Cu
VNSP049A	+++	n. d.	(-)	n. d.	n. d.	+	n. d.	+	Zn	Cu
VNSP050A	+++	n. d.	(-)	n. d.	n. d.	+	n. d.	+	Zn	Cu
VNSP051A	+++	n. d.	(-)	n. d.	n. d.	+	n. d.	+	Zn; Bi	Cu
VNSP052A	+++	n. d.	(-)	n. d.	n. d.	+	(-)	+	Zn	Cu
VNSP053A	+++	n. d.	+	n. d.	n. d.	+	(-)	+	Zn	Cu+As
VNSP054A	+++	n. d.	n. d.	n. d.	n. d.	+	(-)	+	Zn	Cu
VNSP055A	+++	n. d.	n. d.	n. d.	n. d.	+	(-)	+	Zn	Cu
VNSP056A	+++	n. d.	(-)	n. d.	n. d.	+	(-)	+	Zn	Cu
VNSP057A	+++	n. d.	(-)	n. d.	n. d.	+	(-)	+	Zn	Cu
VNSP058A	+++	n. d.	(-)	n. d.	n. d.	+	(-)	+	Zn	Cu
VNSP059A	+++	n. d.	+	n. d.	n. d.	+	(-)	+	Zn	Cu+As
VNSP060A	+++	n. d.	+	n. d.	n. d.	+	(-)	(-)	Zn	Cu+As

Artefact	Semi-quantitative elemental composition (EDXRF)									Obs.
	Cu	Sn	As	Sb	Pb	Fe	Ni	Ca	Elem. (-)	
VNSP061A	+++	n. d.	n. d.	n. d.	n. d.	+	(-)	+	Zn	Cu
VNSP062A	+++	n. d.	n. d.	n. d.	n. d.	+	(-)	n. d.	Zn	Cu
VNSP063A	+++	n. d.	(-)	n. d.	n. d.	+	(-)	+	Zn	Cu
VNSP064A	+++	n. d.	(-)	n. d.	n. d.	+	(-)	+	Zn	Cu
VNSP065A	+++	n. d.	(-)	n. d.	n. d.	+	(-)	+	Zn	Cu
VNSP066A	+++	n. d.	(-)	n. d.	n. d.	+	(-)	+	Zn	Cu
VNSP067A	+++	n. d.	n. d.	n. d.	n. d.	+	n. d.	n. d.	Zn	Cu
VNSP068A	+++	n. d.	n. d.	n. d.	n. d.	+	(-)	+	Zn	Cu
VNSP069A	+++	n. d.	(-)	n. d.	n. d.	+	(-)	(-)	Zn	Cu
VNSP070A	+++	n. d.	(-)	n. d.	n. d.	+	(-)	+	Zn	Cu
VNSP071A	+++	n. d.	+	n. d.	n. d.	+	(-)	+	Zn	Cu+As
VNSP072A	+++	n. d.	+	n. d.	n. d.	+	(-)	+	Zn	Cu+As
VNSP073A	+++	n. d.	(-)	n. d.	n. d.	+	(-)	(-)	Zn	Cu
VNSP074A	+++	n. d.	(-)	n. d.	n. d.	+	(-)	+	Zn	Cu
VNSP075A	+++	n. d.	+	n. d.	n. d.	+	+	+	Zn	Cu+As
VNSP076A	+++	n. d.	(-)	n. d.	n. d.	+	(-)	+	Zn	Cu
VNSP077A	+++	n. d.	(-)	n. d.	n. d.	+	(-)	+	Zn	Cu
VNSP078A	+++	n. d.	(-)	+	n. d.	+	(-)	+	Zn	Cu
VNSP079A	+++	n. d.	(-)	n. d.	n. d.	+	(-)	+	Zn	Cu
VNSP080A	+++	n. d.	(-)	n. d.	n. d.	+	(-)	+	Zn	Cu
VNSP081A	+++	n. d.	(-)	n. d.	n. d.	+	(-)	+	Zn	Cu
VNSP082A	+++	n. d.	(-)	n. d.	n. d.	+	(-)	+	Zn	Cu
VNSP083A	+++	n. d.	n. d.	n. d.	n. d.	+	n. d.	+	Zn	Cu
VNSP084A	+++	n. d.	n. d.	n. d.	n. d.	+	n. d.	+	Zn	Cu
VNSP085A	+++	n. d.	(-)	n. d.	n. d.	+	(-)	+	Zn	Cu
VNSP086A	+++	n. d.	(-)	n. d.	n. d.	+	(-)	+	Zn	Cu
VNSP087A	+++	n. d.	n. d.	n. d.	n. d.	+	(-)	+	Zn	Cu
VNSP088A	+++	n. d.	(-)	n. d.	n. d.	+	(-)	+	Zn	Cu
VNSP089A	+++	n. d.	n. d.	n. d.	n. d.	+	(-)	+	Zn	Cu
VNSP090A	+++	n. d.	n. d.	n. d.	n. d.	+	(-)	+	Zn	Cu
VNSP091A	+++	n. d.	n. d.	n. d.	n. d.	+	(-)	(-)	Zn	Cu
VNSP092A	+++	n. d.	(-)	n. d.	n. d.	+	(-)	(-)	Zn	Cu
VNSP093A	+++	n. d.	(-)	n. d.	n. d.	+	(-)	(-)	Zn	Cu
VNSP094A	+++	n. d.	(-)	n. d.	n. d.	+	(-)	+	Zn	Cu
VNSP095A	+++	n. d.	n. d.	n. d.	n. d.	+	(-)	+	Zn	Cu
VNSP096A	+++	n. d.	+	n. d.	n. d.	+	(-)	+	Zn	Cu+As
VNSP097A	+++	n. d.	++	n. d.	n. d.	+	(-)	+	Zn	Cu
VNSP098A	+++	n. d.	n. d.	n. d.	n. d.	+	(-)	+	Zn	Cu
VNSP099A	+++	n. d.	n. d.	n. d.	n. d.	+	(-)	+	Zn	Cu
VNSP100A	+++	n. d.	n. d.	n. d.	n. d.	+	(-)	+	Zn	Cu
VNSP101A	+++	n. d.	(-)	n. d.	n. d.	+	(-)	+	Zn	Cu
VNSP102A	+++	n. d.	n. d.	n. d.	n. d.	+	(-)	+	Zn	Cu
VNSP103A	+++	n. d.	(-)	n. d.	n. d.	+	(-)	(-)	Zn	Cu
VNSP104A	+++	n. d.	+	n. d.	n. d.	(-)	(-)	+	Zn	Cu+As
VNSP105A	+++	n. d.	++	n. d.	n. d.	(-)	(-)	+	Zn	Cu
VNSP106A	+++	n. d.	(-)	n. d.	n. d.	(-)	(-)	+	Zn	Cu
VNSP107A	+++	n. d.	(-)	n. d.	n. d.	(-)	(-)	(-)	Zn	Cu
VNSP108A	+++	n. d.	n. d.	n. d.	n. d.	(-)	(-)	+	Zn	Cu
VNSP109A	+++	n. d.	n. d.	n. d.	n. d.	(-)	(-)	+	Zn	Cu
VNSP110A	+++	n. d.	(-)	n. d.	n. d.	(-)	(-)	(-)	Zn	Cu
VNSP111A	+++	n. d.	n. d.	n. d.	n. d.	(-)	(-)	(-)	Zn	Cu
VNSP112A	+++	n. d.	(-)	n. d.	n. d.	(-)	(-)	(-)	Zn	Cu
VNSP113A	+++	n. d.	(-)	n. d.	n. d.	(-)	(-)	+	Zn	Cu
VNSP114A	+++	n. d.	(-)	n. d.	n. d.	(-)	(-)	+	Zn	Cu
VNSP115A	+++	n. d.	+	n. d.	n. d.	(-)	(-)	+	Zn	Cu+As
VNSP116A	+++	++	n. d.	n. d.	n. d.	(-)	(-)	+	Zn	Cu+Sn
VNSP117A	+++	n. d.	n. d.	n. d.	n. d.	+	(-)	(-)	Zn	Cu
VNSP118A	+++	n. d.	n. d.	n. d.	n. d.	(-)	(-)	+	Zn	Cu
VNSP119A	+++	n. d.	+	n. d.	n. d.	+	(-)	+	Zn	Cu+As
VNSP120A	+++	n. d.	(-)	n. d.	n. d.	(-)	(-)	+	Zn	Cu
VNSP121A	+++	n. d.	(-)	n. d.	n. d.	(-)	(-)	+	Zn	Cu
VNSP122A	+++	++	(-)	n. d.	n. d.	(-)	(-)	+	Zn	Cu+Sn
VNSP123B	+++	n. d.	n. d.	n. d.	n. d.	+	n. d.	+	Zn	Cu
VNSP124B	+++	n. d.	(-)	n. d.	n. d.	+	(-)	+	Zn	Cu
VNSP125B	+++	n. d.	+	n. d.	n. d.	+	(-)	+	Zn	Cu+As
VNSP126B	+++	n. d.	+	n. d.	n. d.	+	(-)	+	Zn; Bi↓	Cu+As
VNSP127B	+++	n. d.	n. d.	n. d.	n. d.	+	(-)	+	Zn	Cu
VNSP128B	+++	n. d.	+	n. d.	n. d.	+	(-)	+	Zn	Cu+As

Artefact	Semi-quantitative elemental composition (EDXRF)									Obs.
	Cu	Sn	As	Sb	Pb	Fe	Ni	Ca	Elem. (-)	
VNSP129B	+++	n. d.	n. d.	n. d.	n. d.	+	(-)	+	Zn	Cu
VNSP130B	+++	n. d.	+	n. d.	n. d.	+	(-)	+	Zn	Cu+As
VNSP131B	+++	n. d.	n. d.	n. d.	n. d.	+	(-)	+	Zn	Cu
VNSP132C	+++	n. d.	+	n. d.	n. d.	+	(-)	+	Zn	Cu+As
VNSP133C	+++	n. d.	+	(-)	n. d.	+	n. d.	+	Zn	Cu+As
VNSP134C	+++	n. d.	n. d.	n. d.	n. d.	+	n. d.	+	Zn	Cu
VNSP135C	+++	n. d.	+	n. d.	n. d.	+	(-)	+	Zn; Bi	Cu+As
VNSP136C	+++	n. d.	n. d.	(-)	n. d.	+	(-)	+	Zn	Cu
VNSP137C	+++	n. d.	n. d.	n. d.	n. d.	+	(-)	+	Zn	Cu
VNSP138C	+++	n. d.	+	n. d.	n. d.	+	(-)	+	Zn	Cu+As
VNSP139C	+++	n. d.	+	n. d.	n. d.	+	n. d.	+	Zn	Cu+As
VNSP140C	+++	n. d.	+	n. d.	n. d.	+	(-)	+	Zn	Cu+As
VNSP141C	+++	n. d.	+	n. d.	n. d.	(-)	(-)	(-)	Zn	Cu+As
VNSP142C	+++	n. d.	(-)	n. d.	n. d.	+	n. d.	(-)	Zn	Cu
VNSP143C	+++	n. d.	+	n. d.	n. d.	+	(-)	+	Zn	Cu+As
VNSP144D	+++	n. d.	n. d.	n. d.	n. d.	+	n. d.	+	Zn	Cu
VNSP145D	+++	n. d.	n. d.	n. d.	n. d.	+	n. d.	+	Zn	Cu
VNSP146D	+++	n. d.	+	n. d.	n. d.	(-)	n. d.	+	Zn	Cu+As
VNSP147D	+++	n. d.	+	n. d.	n. d.	+	(-)	+	Zn	Cu+As
VNSP148D	+++	n. d.	++	n. d.	n. d.	+	n. d.	+	Zn	Cu+As↑
VNSP149D	+++	n. d.	+	n. d.	n. d.	+	n. d.	+	Zn	Cu+As
VNSP150D	+++	n. d.	(-)	n. d.	n. d.	+	n. d.	+	Zn	Cu
VNSP151D	+++	n. d.	(-)	n. d.	n. d.	+	(-)	+	Zn	Cu
VNSP152D	+++	n. d.	n. d	n. d.	n. d.	+	n. d.	+	Zn	Cu
VNSP153D	+++	n. d.	+	n. d.	n. d.	+	n. d.	+	Zn	Cu+As
VNSP154D	+++	n. d.	+	n. d.	n. d.	+	n. d.	+	Zn	Cu+As
VNSP155D	+++	n. d.	(-)	n. d.	n. d.	+	n. d.	+	Zn	Cu
VNSP156D	+++	n. d.	+	++	n. d.	+	n. d.	+	Zn; Bi↓	Cu+As
VNSP157D	+++	n. d.	+	n. d.	n. d.	+	n. d.	+	Zn	Cu+As
VNSP158D	+++	n. d.	+	n. d.	n. d.	+	n. d.	+	Zn	Cu+As
VNSP159D	+++	n. d.	n. d.	n. d.	n. d.	+	n. d.	+	Zn	Cu
VNSP160D	+++	n. d.	n. d.	n. d.	n. d.	+	n. d.	+	Zn	Cu
VNSP161D	+++	n. d.	+	n. d.	n. d.	+	n. d.	+	Zn	Cu+As
VNSP162D	+++	n. d.	n. d.	n. d.	n. d.	+	n. d.	+	Zn	Cu
VNSP163D	+++	n. d.	+	n. d.	n. d.	+	n. d.	+	Zn	Cu+As
VNSP164D	+++	n. d.	n. d.	n. d.	n. d.	+	n. d.	+	Zn	Cu
VNSP165D	+++	n. d.	+	n. d.	n. d.	+	(-)	+	Zn	Cu+As
VNSP166D	+++	n. d.	+	n. d.	n. d.	+	(-)	+	Zn	Cu+As
VNSP167D	+++	n. d.	+	n. d.	n. d.	+	(-)	+	Zn	Cu+As
VNSP168D	+++	n. d.	+	n. d.	n. d.	+	(-)	+	Zn	Cu+As
VNSP169D	+++	n. d.	n. d.	n. d.	n. d.	+	n. d.	+	Zn	Cu
VNSP170D	+++	n. d.	+	n. d.	n. d.	+	n. d.	+	Zn	Cu+As
VNSP171D	+++	n. d.	+	n. d.	n. d.	+	(-)	+	Zn	Cu+As
VNSP172D	+++	n. d.	n. d.	n. d.	n. d.	+	(-)	+	Zn	Cu
VNSP173D	+++	n. d.	+	n. d.	n. d.	+	n. d.	+	Zn	Cu+As
VNSP174D	+++	n. d.	(-)	n. d.	n. d.	+	(-)	+	Zn	Cu
VNSP175D	+++	n. d.	+	n. d.	n. d.	+	(-)	+	Zn	Cu+As
VNSP176D	+++	n. d.	n. d.	n. d.	n. d.	+	n. d.	+	Zn	Cu
VNSP178D	+++	n. d.	+	n. d.	(-)	+	n. d.	+	Zn	Cu+As
VNSP179E	+++	++(+)	+	n. d.	(-)	+	n. d.	+	Zn	Cu+Sn
VNSP180E	+++	n. d.	++	n. d.	n. d.	+	n. d.	+	Zn	Cu+As↑
VNSP181E	+++	n. d.	+	n. d.	n. d.	+	n. d.	+	Zn	Cu+As
VNSP182E	+++	n. d.	+	n. d.	n. d.	+	n. d.	+	Zn	Cu+As
VNSP183E	+++	n. d.	++	n. d.	n. d.	+	n. d.	+	Zn	Cu+As↑
VNSP185F	+++	n. d.	(-)	n. d.	n. d.	+	n. d.	+	Zn	Cu
VNSP186F	+++	n. d.	n. d.	n. d.	n. d.	+	n. d.	+	Zn	Cu
VNSP187F	+++	n. d.	n. d.	n. d.	n. d.	+	n. d.	+	Zn	Cu
VNSP177G	+++	n. d.	+	n. d.	(-)	+	n. d.	+	Zn	Cu+As
VNSP188G	+++	n. d.	+	n. d.	n. d.	(-)	n. d.	+	Zn	Cu+As
VNSP189G	+++	n. d.	++	n. d.	n. d.	+	n. d.	+	Zn	Cu+As↑
VNSP190H	+++	n. d.	+	n. d.	n. d.	+	n. d.	+	Zn	Cu+As
VNSP025I	+++	n. d.	+	n. d.	n. d.	+	(-)	+	Zn	Cu+As
VNSP184I	+++	n. d.	+	n. d.	n. d.	+	n. d.	+	Zn	Cu+As
VNSP191I	+++	n. d.	++	n. d.	n. d.	+	n. d.	+	Zn	Cu+As↑
VNSP192I	+++	n. d.	+	n. d.	n. d.	+	n. d.	+	Zn	Cu+As
VNSP193I	+++	n. d.	(-)	n. d.	n. d.	(-)	(-)	+	Zn	Cu
VNSP194I	+++	n. d.	(-)	n. d.	n. d.	(-)	(-)	+	Zn	Cu
VNSP195I	+++	n. d.	n. d.	n. d.	n. d.	+	(-)	+	Zn	Cu

Artefact	Semi-quantitative elemental composition (EDXRF)									Obs.
	Cu	Sn	As	Sb	Pb	Fe	Ni	Ca	Elem. (-)	
VNSP196I	+++	n. d.	(-)	n. d.	n. d.	(-)	(-)	+	Zn	Cu
VNSP197I	+++	n. d.	(-)	n. d.	n. d.	+	(-)	+	Zn	Cu
VNSP198I	+++	n. d.	(-)	n. d.	n. d.	(-)	(-)	(-)	Zn	Cu
VNSP199I	+++	n. d.	+	n. d.	n. d.	+	(-)	+	Zn	Cu+As
VNSP200I	+++	n. d.	+	n. d.	n. d.	+	(-)	+	Zn	Cu+As
VNSP201I	+++	n. d.	(-)	n. d.	n. d.	(-)	(-)	(-)	Zn	Cu
VNSP202I	+++	n. d.	(-)	n. d.	n. d.	+	(-)	+	Zn	Cu
VNSP203I	+++	n. d.	(-)	n. d.	n. d.	(-)	(-)	+	Zn; Bi↓	Cu
VNSP204I	+++	n. d.	+	n. d.	n. d.	+	(-)	+	Zn	Cu+As
VNSP205I	+++	n. d.	n. d.	n. d.	n. d.	(-)	(-)	+	Zn	Cu
VNSP206I	+++	n. d.	(-)	n. d.	n. d.	(-)	(-)	+	Zn	Cu
VNSP207I	+++	n. d.	(-)	n. d.	n. d.	+	(-)	+	Zn	Cu
VNSP208I	+++	n. d.	n. d.	n. d.	n. d.	(-)	(-)	+	Zn	Cu
VNSP209I	+++	n. d.	n. d.	n. d.	n. d.	(-)	(-)	+	Zn	Cu
VNSP210I	+++	n. d.	(-)	n. d.	n. d.	(-)	(-)	+	Zn	Cu
VNSP211I	+++	n. d.	(-)	n. d.	n. d.	(-)	(-)	+	Zn	Cu
VNSP212I	+++	n. d.	(-)	n. d.	n. d.	(-)	(-)	+	Zn	Cu
VNSP213I	+++	n. d.	n. d.	n. d.	n. d.	+	(-)	+	Zn	Cu
VNSP214I	+++	n. d.	(-)	n. d.	n. d.	(-)	(-)	+	Zn	Cu
VNSP215I	+++	n. d.	(-)	n. d.	n. d.	(-)	(-)	+	Zn	Cu
VNSP216I	+++	n. d.	(-)	n. d.	n. d.	(-)	(-)	+	Zn	Cu
VNSP217I	+++	n. d.	(-)	n. d.	n. d.	(-)	(-)	+	Zn; Bi	Cu
VNSP218I	+++	n. d.	(-)	n. d.	n. d.	(-)	(-)	+	Zn	Cu
VNSP219I	+++	n. d.	(-)	n. d.	n. d.	(-)	(-)	(-)	Zn; Bi	Cu
VNSP220I	+++	n. d.	(-)	n. d.	n. d.	+	(-)	+	Zn; Bi	Cu
VNSP221I	+++	n. d.	(-)	n. d.	n. d.	(-)	(-)	+	Zn	Cu
VNSP222I	+++	n. d.	(-)	+	n. d.	(-)	(-)	+	Zn	Cu
VNSP223I	+++	n. d.	(-)	n. d.	n. d.	+	(-)	+	Zn; Bi↓	Cu
VNSP224I	+++	n. d.	++	+	n. d.	+	(-)	+	Zn; Bi	Cu+As↑
VNSP225I	+++	n. d.	(-)	n. d.	n. d.	+	(-)	+	Zn; Bi	Cu
VNSP226I	+++	n. d.	(-)	n. d.	n. d.	(-)	(-)	+	Zn; Bi	Cu+As
VNSP227I	+++	n. d.	(-)	n. d.	n. d.	(-)	(-)	+	Zn	Cu
VNSP228I	+++	n. d.	(-)	n. d.	n. d.	(-)	(-)	+	Zn	Cu
VNSP229I	+++	n. d.	(-)	n. d.	n. d.	(-)	(-)	+	Zn	Cu
VNSP230I	+++	n. d.	n. d.	n. d.	n. d.	(-)	(-)	+	Zn	Cu
VNSP231I	+++	n. d.	(-)	n. d.	n. d.	(-)	(-)	+	Zn	Cu
VNSP232I	+++	n. d.	(-)	n. d.	n. d.	(-)	(-)	+	Zn	Cu
VNSP233I	+++	n. d.	+	n. d.	n. d.	+	(-)	+	Zn; Bi	Cu+As
VNSP234I	+++	n. d.	(-)	n. d.	n. d.	+	(-)	+	Zn; Bi	Cu
VNSP235I	+	n. d.	n. d.	n. d.	n. d.	++	(-)	+	Zn; Rb; Sr	Fe
VNSP236I	+++	n. d.	(-)	n. d.	n. d.	+	(-)	+	Zn	Cu
VNSP237I	+++	n. d.	(-)	n. d.	n. d.	+	(-)	+	Zn	Cu
VNSP238I	+++	n. d.	(-)	n. d.	n. d.	(-)	(-)	+	Zn	Cu
VNSP239I	+++	n. d.	+	n. d.	n. d.	(-)	(-)	+	Zn	Cu+As
VNSP240I	+++	n. d.	(-)	n. d.	n. d.	(-)	(-)	+	Zn	Cu
VNSP241I	+++	n. d.	(-)	n. d.	n. d.	(-)	(-)	+	Zn	Cu
VNSP242I	+++	n. d.	n. d.	n. d.	n. d.	(-)	(-)	+	Zn	Cu
VNSP243I	+++	n. d.	(-)	n. d.	n. d.	(-)	(-)	+	Zn	Cu
VNSP244I	+++	n. d.	+	n. d.	n. d.	+	(-)	+	Zn	Cu+As
VNSP245I	+++	n. d.	(-)	n. d.	n. d.	+	(-)	+	Zn	Cu
VNSP246I	+++	n. d.	(-)	n. d.	n. d.	(-)	(-)	+	Zn	Cu
VNSP247I	+++	n. d.	n. d.	n. d.	n. d.	(-)	(-)	+	Zn	Cu
VNSP248I	+++	n. d.	(-)	n. d.	n. d.	(-)	(-)	+	Zn	Cu
VNSP249I	+++	n. d.	(-)	n. d.	n. d.	(-)	(-)	+	Zn	Cu
VNSP250I	+++	n. d.	+	n. d.	n. d.	(-)	(-)	+	Zn	Cu+As
VNSP251I	+++	n. d.	(-)	n. d.	n. d.	+	(-)	+	Zn	Cu
VNSP252I	+++	n. d.	+ (+)	n. d.	n. d.	+	(-)	+	Zn	Cu+As
VNSP253I	+++	n. d.	(-)	n. d.	n. d.	(-)	(-)	+	Zn	Cu
VNSP254I	+++	n. d.	(-)	n. d.	n. d.	(-)	(-)	+	Zn	Cu
VNSP255I	+++	n. d.	n. d.	n. d.	n. d.	(-)	(-)	+	Zn	Cu
VNSP256I	+++	n. d.	(-)	n. d.	n. d.	(-)	(-)	+	Zn	Cu
VNSP257I	+++	n. d.	(-)	n. d.	n. d.	(-)	(-)	+	Zn	Cu
VNSP258I	+++	n. d.	(-)	n. d.	n. d.	(-)	(-)	+	Zn	Cu
VNSP259I	+++	n. d.	(-)	n. d.	n. d.	+	(-)	+	Zn	Cu
VNSP260I	(-)	n.d.	n. d.	n. d.	n. d.	+++	n. d.	(-)	Zn	Fe
VNSP261C	+++	n.d.	+	n.d.	n.d.	++	n.d.	+	Bi	Cu+As
VNSP262C	+++	n.d.	n.d.	n.d.	n.d.	++	n.d.	+	n.d.	Cu

Artefact	Semi-quantitative elemental composition (EDXRF)									Obs.
	Cu	Sn	As	Sb	Pb	Fe	Ni	Ca	Elem. (-)	
VNSP263C	+++	n.d.	+	n.d.	n.d.	++	n.d.	++	n.d.	Cu+As
VNSP264C	+++	n.d.	+	n.d.	n.d.	+	n.d.	+	n.d.	Cu+As
VNSP265C	+++	n.d.	+	n.d.	n.d.	+	n.d.	+	n.d.	Cu+As
VNSP266C	+++	n.d.	(-)	n.d.	n.d.	+	n.d.	+	n.d.	Cu
VNSP267D	+++	n.d.	(-)	n.d.	n.d.	+	n.d.	++	n.d.	Cu
VNSP268D	+++	n.d.	n.d.	n.d.	n.d.	+	n.d.	+	n.d.	Cu
VNSP269D	+++	n.d.	n.d.	n.d.	n.d.	+	n.d.	(-)	n.d.	Cu
VNSP270D	+++	n.d.	+	n.d.	n.d.	+	n.d.	+	n.d.	Cu+As
VNSP271D	+++	n.d.	++	n.d.	n.d.	+	n.d.	n.d.	n.d.	Cu+As↑
VNSP272D	+++	n.d.	++	n.d.	n.d.	++	n.d.	(-)	n.d.	Cu+As↑
VNSP273D	+++	n.d.	n.d.	n.d.	n.d.	+	n.d.	n.d.	n.d.	Cu
VNSP274D	+++	n.d.	++	n.d.	n.d.	+	n.d.	n.d.	n.d.	Cu+As↑
VNSP275D	+++	n.d.	++	n.d.	n.d.	+	n.d.	+	n.d.	Cu+As↑

Appendix III – Summary of general characteristics of VNSP artefacts

Table III.1. Summary of sampling and general MO micrographies observations (BF) of: A - Awls and B - Wires.

VNSP001A	VNSP021A	VNSP023A
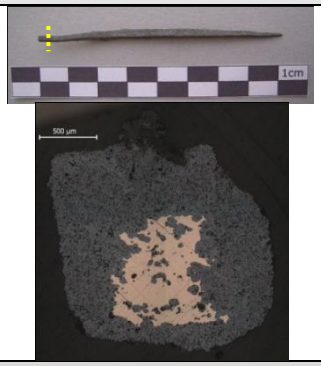		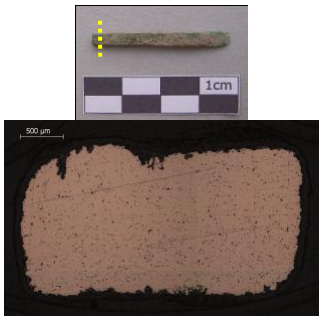
VNSP029A	**VNSP031A**	**VNSP038A**
		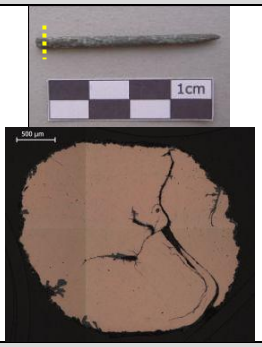
VNSP040A	**VNSP047A**	**VNSP049A**
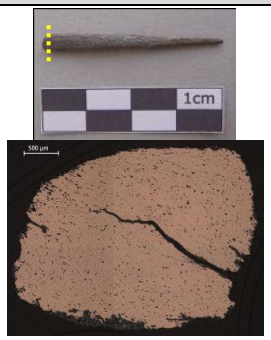	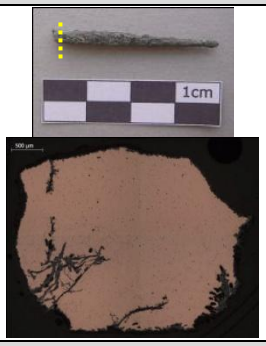	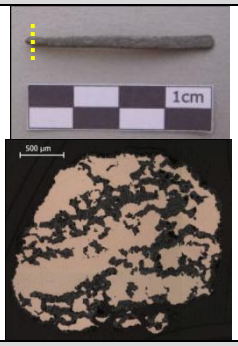
VNSP097A	**VNSP123B**	**VNSP124B**
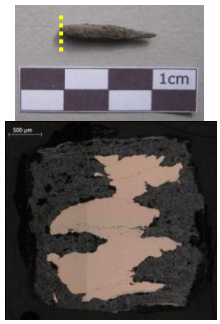	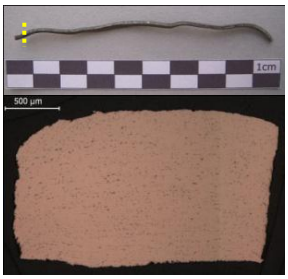	

Table III.2. Summary of sampling and general MO micrographies observations (BF) of: C – Chisels.

VNSP132C	VNSP133C	VNSP134C
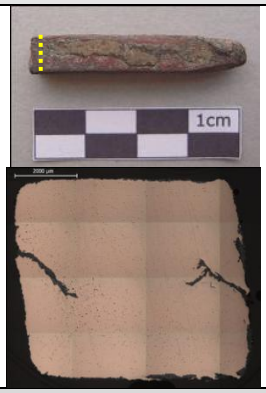	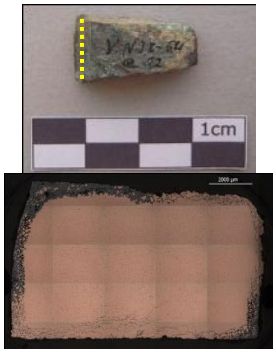	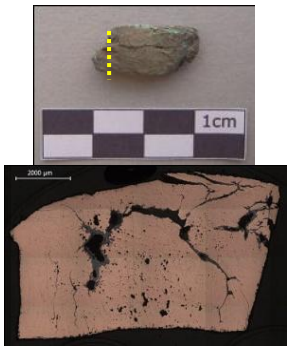
VNSP135C	**VNSP136C**	**VNSP137C**
	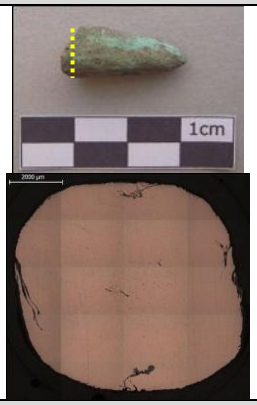	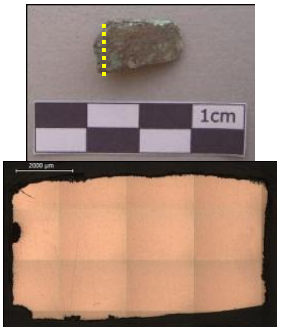
VNSP138C	**VNSP139C**	**VNSP140C**
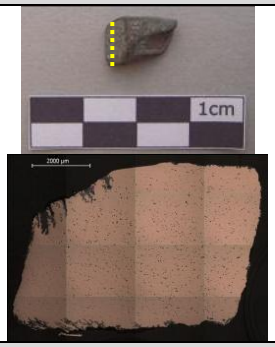	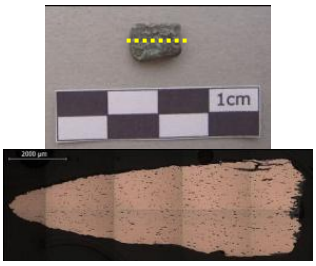	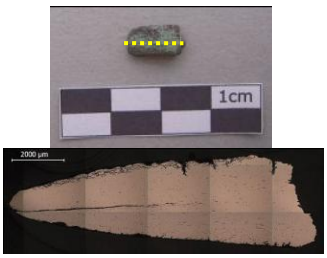
VNSP141C	**VNSP262C**	
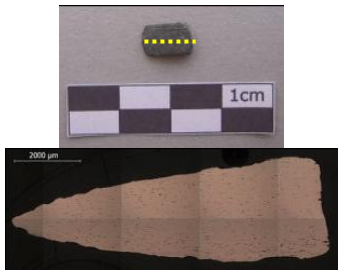	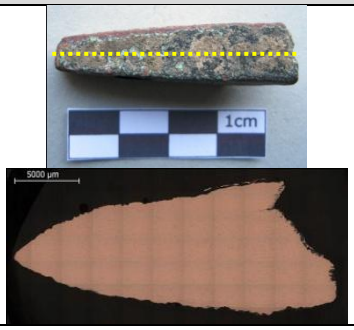	

Table III.3. Summary of sampling and general MO micrographies observations (BF) of: D – Axes.

* Same artefact cut in two directions - Longitudinal and Transversal.

VNSP144D	VNSP145DT*	VNSP145DL*
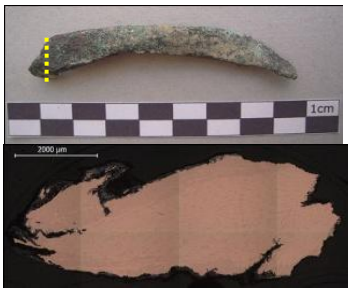		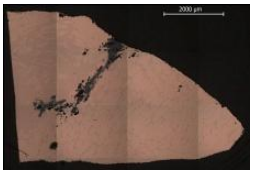
VNSP146D	**VNSP147D**	**VNSP148D**
		
VNSP150D	**VNSP153D**	**VNSP154D**
		
VNSP155D	**VNSP165D**	**VNSP178D**
		
VNSP268D		
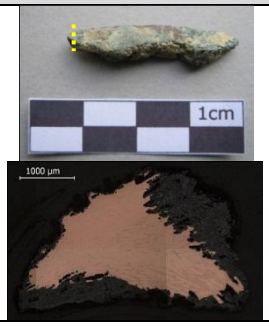		

Table III.4. Summary of sampling and general MO micrographies observations (BF) of: E – Blades, Arrowheads.

VNSP180E	VNSP181E	VNSP182E
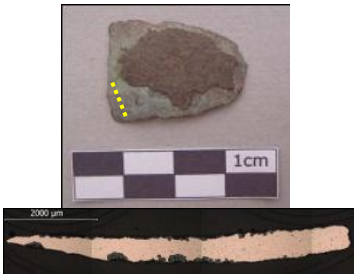		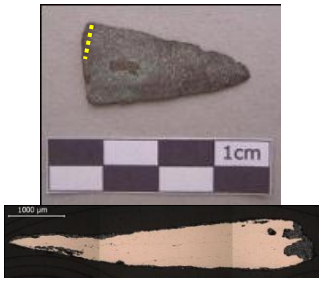

VNSP183E
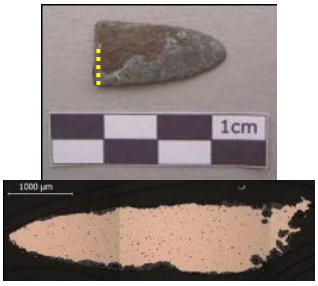

Table III.5. Summary of sampling and general MO micrographies observations (BF) of: F – Saws.

VNSP185F	VNSP186F	VNSP187F
		

Table III.6. Summary of sampling and general MO micrographies observations (BF) of: G – Daggers.

VNSP177G	VNSP188G	VNSP189G
		

Table III.7. Summary of sampling and general MO micrographies observations (BF) of: H – Socket.

VNSP190H
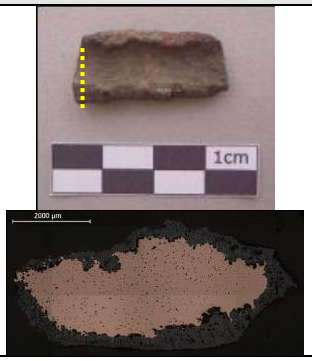

Table III.8. Summary of sampling and general MO micrographies observations (BF) of: I – Indeterminates.

VNSP025I	VNSP184I	VNSP191I
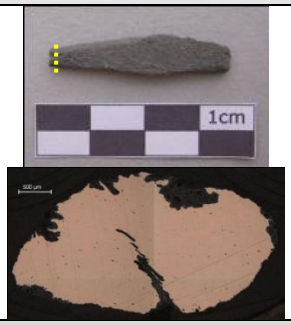		
VNSP192I	**VNSP193I**	**VNSP194I**
	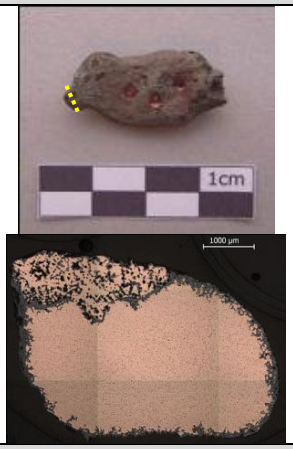	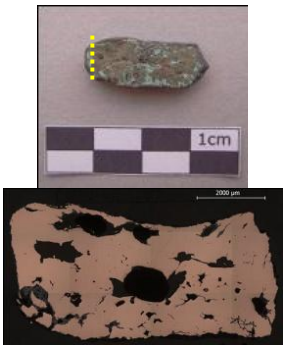

VNSP196I


Appendix IV – Summary of Micro-EDXRF experimental results

Table IV.1. Summary of Micro-EDXRF experimental results (%) of selected artefacts from VNSP.

Composition of the alloy is given by average of three determinations per artefact; <0.07% As, <0.05 Fe% - under detection limit; * Artefact observed in two sections - Longitudinal and Transversal.

		Elements identified and quantified (%)		
Typologies	**Artefacts**	**Cu**	**As**	**Fe**
A - Awls	VNSP001A	95.43	4.36	<0.05
	VNSP021A	98.90	0.90	<0.05
	VNSP023A	98.73	0.96	<0.05
	VNSP029A	96.53	3.19	<0.05
	VNSP031A	98.27	1.43	<0.05
	VNSP038A	98.10	1.56	0.07
	VNSP040A	96.30	3.39	0.05
	VNSP047A	99.70	<0.07	<0.05
	VNSP049A	94.17	5.59	<0.05
	VNSP097A	93.70	6.04	<0.05
B - Wires	VNSP123B	99.50	0.21	<0.05
	VNSP124B	99.60	0.19	<0.05
C - Chisels	VNSP132C	94.87	4.92	<0.05
	VNSP133C	99.50	0.27	<0.05
	VNSP134C	99.70	<0.07	<0.05
	VNSP135C	98.23	1.53	<0.05
	VNSP136C	99.73	<0.07	<0.05
	VNSP137C	99.77	<0.07	<0.05
	VNSP138C	98.73	1.08	<0.05
	VNSP139C	98.07	1.71	<0.05
	VNSP140C	96.33	3.43	<0.05
	VNSP141C	97.17	2.61	<0.05
	VNSP262C	99.82	<0.07	<0.05
D - Axes	VNSP144D	99.73	<0.07	0.21
	VNSP145D T*	99.80	<0.07	<0.05
	VNSP145D L*	99.50	<0.07	<0.05
	VNSP146D	97.73	2.04	<0.05
	VNSP147D	97.93	1.85	<0.05
	VNSP148D	90.57	9.13	0.07
	VNSP150D	99.50	0.24	<0.05
	VNSP153D	98.63	1.08	0.05
	VNSP154D	98.20	1.58	<0.05
	VNSP155D	98.90	0.79	<0.05
	VNSP165D	98.37	1.42	<0.05
	VNSP178D	99.70	<0.07	<0.05
	VNSP268D	99.79	<0.07	<0.05
E – Blades,	VNSP180E	94.17	5.57	<0.05
Arrowheads	VNSP181E	97.53	2.22	<0.05
	VNSP182E	94.10	5.66	<0.05
	VNSP183E	95.83	3.89	<0.05
F - Saws	VNSP185F	99.70	0.09	<0.05
	VNSP186F	99.73	<0.07	<0.05
	VNSP187F	99.77	<0.07	<0.05
G - Daggers	VNSP177G	99.80	<0.07	<0.05
	VNSP188G	97.93	1.79	<0.05
	VNSP189G	95.20	4.53	<0.05
H - Socket	VNSP190H	98.17	1.57	<0.05
I - Indeterminate	VNSP025I	96.37	3.37	<0.05
	VNSP184I	96.13	3.85	<0.05
	VNSP191I	94.30	5.49	<0.05
	VNSP192I	96.57	3.13	<0.05
	VNSP193I	97.40	2.32	<0.05
	VNSP194I	99.17	0.51	<0.05
	VNSP196I	98.95	0.86	<0.05

Appendix V – Summary of microstrutural observations of VNSP artefacts

Table V.1. Summary of MO micrographies of: A - Awls and B - Wires.

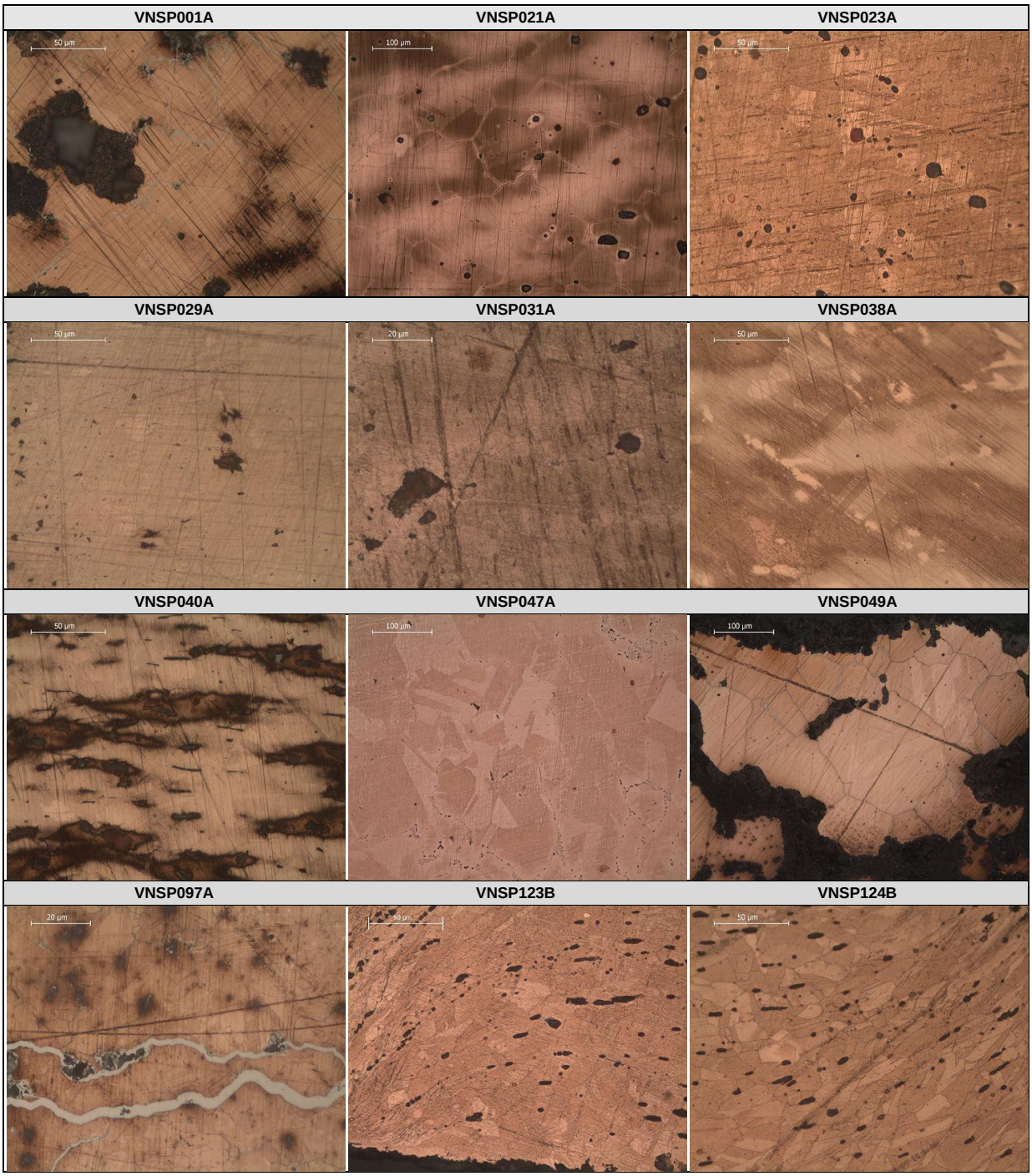

Table V.2. Summary of MO micrographies of: C – Chisels.

VNSP132C	VNSP133C	VNSP134C
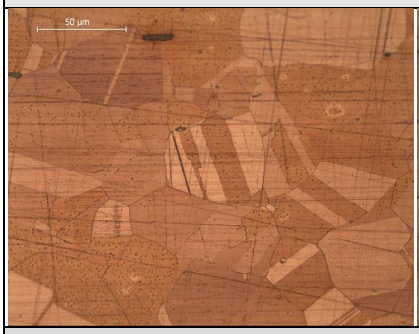	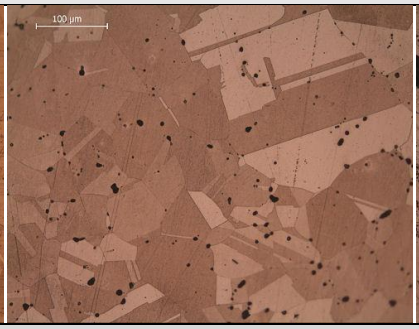	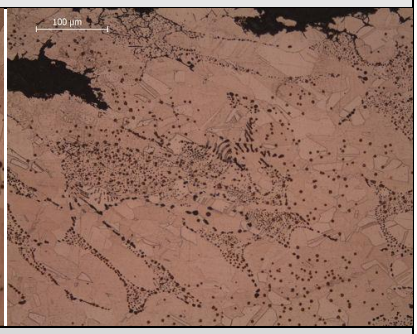
VNSP135C	**VNSP136C**	**VNSP137C**
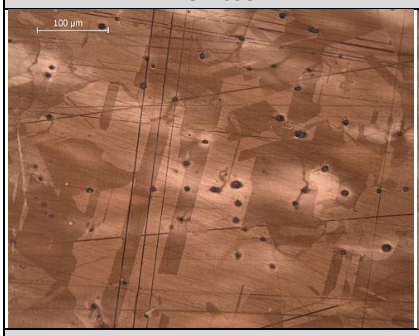	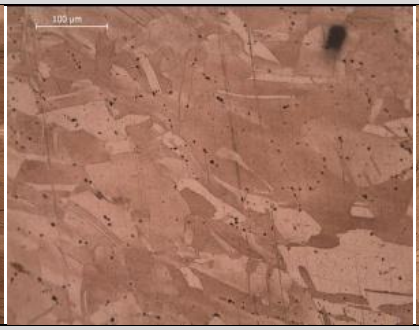	
VNSP138C	**VNSP139C**	**VNSP140C**
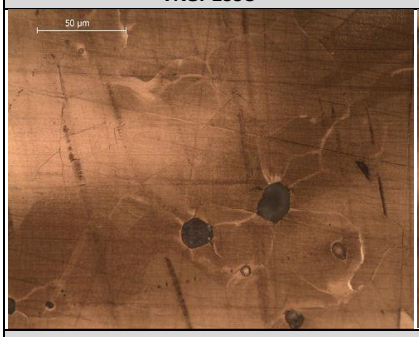		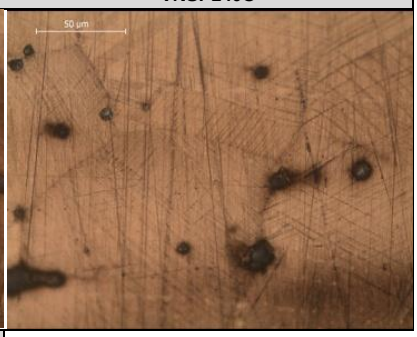
VNSP141C	**VNSP262C**	
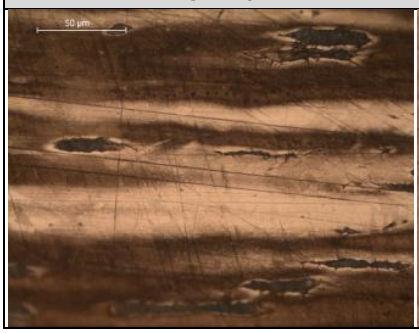		

Table V.3. Summary of MO micrographies of: D – Axes.

* Artefact observed in two sections - Longitudinal and Transversal.

VNSP144D	VNSP145DT*	VNSP145DL*
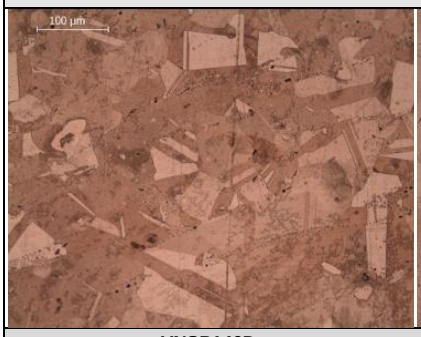		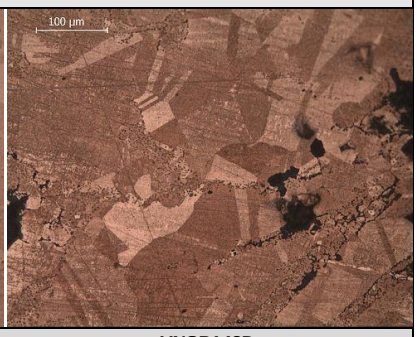
VNSP146D	**VNSP147D**	**VNSP148D**
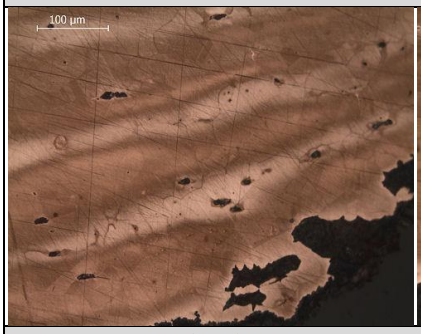	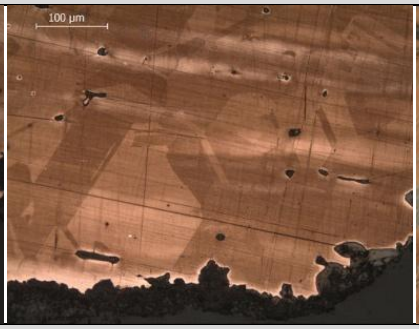	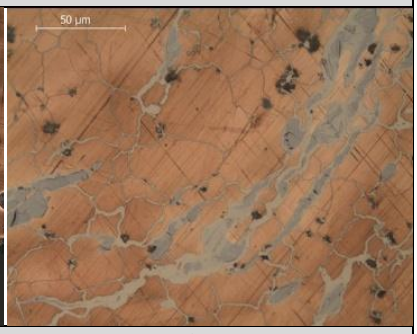
VNSP150D	**VNSP153D**	**VNSP154D**
		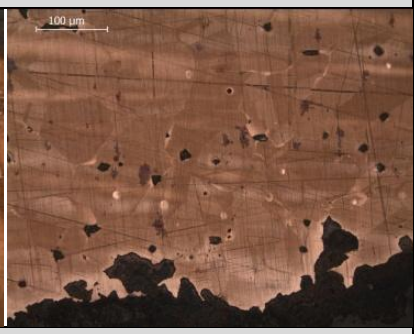
VNSP155D	**VNSP165D**	**VNSP178D**
	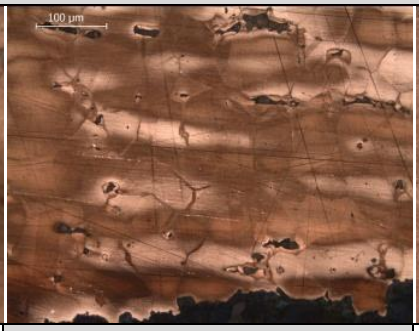	
VNSP268D		
		

Table V.4. Summary of MO micrographies of: E – Blades, Arrowheads.

VNSP180E	VNSP181E	VNSP182E
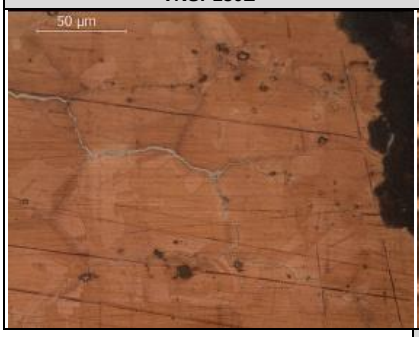	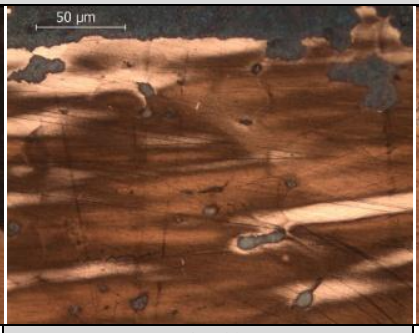	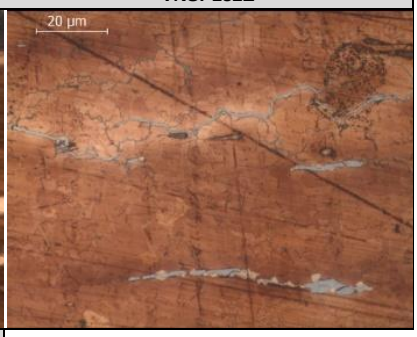

VNSP183E
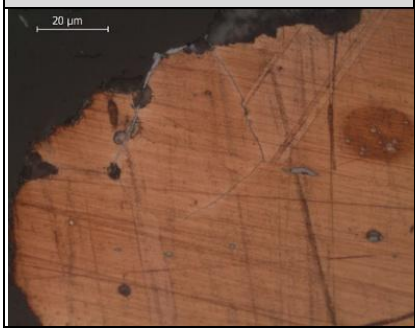

Table V.5. Summary of MO micrographies of: F – Saws.

VNSP185F	VNSP186F	VNSP187F
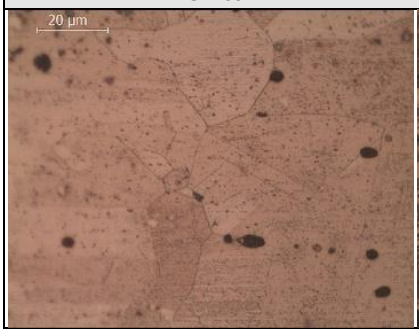	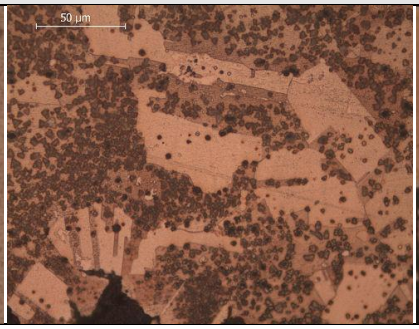	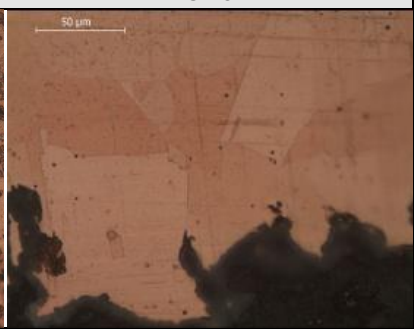

Table V.6. Summary of MO micrographies of: G – Daggers.

VNSP177G	VNSP188G	VNSP189G
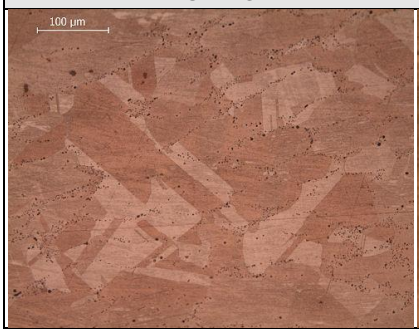		

Table V.7. Summary of MO micrographies of: H – Socket.

VNSP190H


Table V.8. Summary of MO micrographies of: I – Indeterminates.

VNSP025I	VNSP184I	VNSP191I
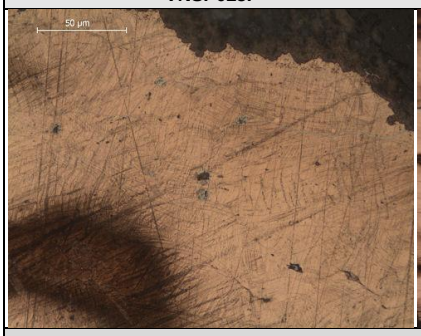	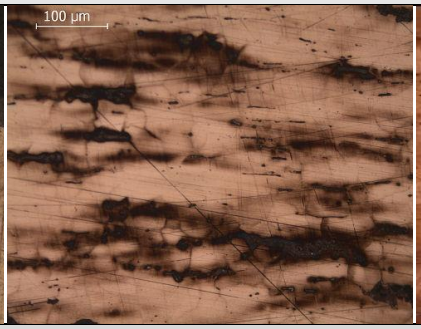	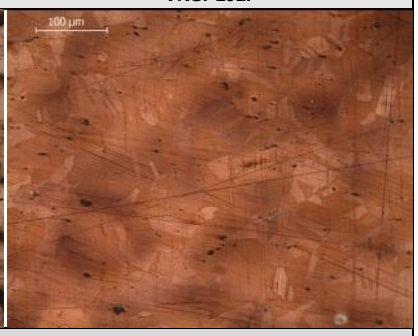
VNSP192I	**VNSP193I**	**VNSP194I**
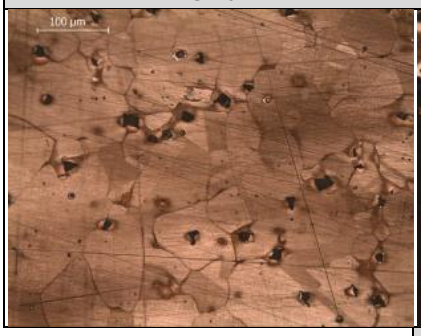	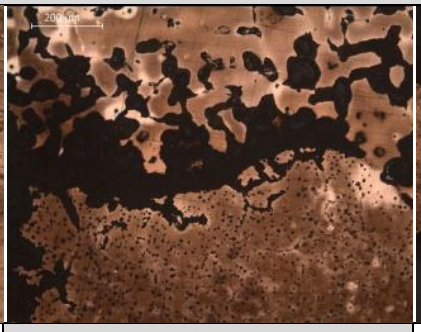	
VNSP196I		
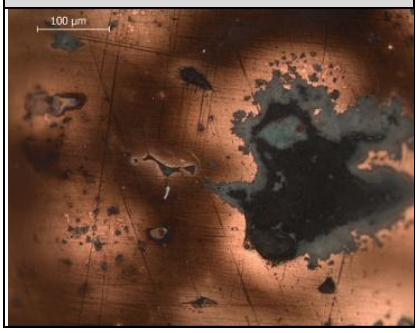		

Appendix VI – Summary of microstrutural characterization of VNSP artefacts

Table VI.1. Microstrutural characterization of selected artefacts from VNSP.

(P: Present; s: segregation bands; t: annealing twins; sb: slip bands; d: deformed inclusions; C: Casting; A: Annealing; F: Forging; FF: Final Forging; ↑: high amount; ↓: low amount; * Samples refers to the same artefact cut in two directions - Longitudinal and Transversal. ** Presenting α-Cu eutetic remains.

Typologies	Artefacts	As (%)	Phases	As (%)	Segregation Cu-As	Inclusions Cu-O	Features	Operatial Sequence
A - Awls	VNSP001A	4,36	α, As-rich	-	P	-	Equiaxial, s, t, sb	C+(F+A)+FF
	VNSP021A	0,90	α	-	-	P (eutectic)	Equiaxial, t, d	C+(F+A)
	VNSP023A	0,96	α	-	-	P	Equiaxial, t	C+(F+A)
	VNSP029A	3,19	α, As-rich	-	P	P	Equiaxial, s, t, d	C+(F+A)
	VNSP031A	1,43	α	-	-	P (eutectic)	Equiaxial, t, d	C+(F+A)
	VNSP038A	1,56	α	-	-	P	Equiaxial, t	C+(F+A)
	VNSP040A	3,39	α	-	-	P (eutectic)	Equiaxial, t, d, sb↓	C+(F+A)+FF↓
	VNSP047A	<0,07	α	-	-	P (eutectic)	Equiaxial, t	C+(F+A)
	VNSP049A	5,59	α, As-rich	-	P	-	Equiaxial, s, t	C+(F+A)
	VNSP097A	6,04	α, As-rich	34,02	P	-	Equiaxial, s, t, sb↓	C+(F+A)+FF↓
B - Wires	VNSP123B	0,21	α	-	-	P (eutectic)	Equiaxial, t, d	C+(F+A)
	VNSP124B	0,19	α	-	-	P (eutectic)	Equiaxial, t, d	C+(F+A)
C – Chisels	VNSP132C	4,92	α, As-rich	-	P	P	Equiaxial, s, t, d?	C+(F+A)
	VNSP133C	0,27	α	-	-	P (eutectic)	Equiaxial, t	C+(F+A)
	VNSP134C	<0,07	α	-	-	P (eutectic)	Equiaxial, t	C+(F+A)
	VNSP135C	1,53	α	-	-	P	Equiaxial, t, d	C+(F+A)
	VNSP136C	<0,07	α	-	-	P (eutectic)	Equiaxial, t, d	C+(F+A)
	VNSP137C	<0,07	α	-	-	P (eutectic)	Equiaxial, t, d, sb↓	C+(F+A)+FF↓
	VNSP138C	1,08	α	-	-	P	Equiaxial, t, d	C+(F+A)
	VNSP139C	1,71	α	-	-	P	Equiaxial, t, d	C+(F+A)
	VNSP140C	3,43	α	-	-	P	Equiaxial, t, d, sb↓	C+(F+A)+FF↓
	VNSP141C	2,61	α	-	-	P	Equiaxial, t, d, sb↓	C+(F+A)+FF↓
	VNSP262C	<0,07	α	-	-	P	Equiaxial, t	C+(F+A)
D – Axes	VNSP144D	<0,07	α	-	-	P	Equiaxial, t	C+(F+A)
	VNSP145D	<0,07	α	-	-	P (eutectic)	Equiaxial, t, d?	C+(F+A)
	VNSP145D	<0,07	α	-	-	P (eutectic)	Equiaxial, t, d?	C+(F+A)
	VNSP146D	2,04	α	-	-	P	Equiaxial, t, d	C+(F+A)
	VNSP147D	1,85	α	-	-	P	Equiaxial, t, d	C+(F+A)
	VNSP148D	9,13	α, As-rich**	34,28	P	-	Equiaxial, s, t	C+(F+A)
	VNSP150D	0,24	α	-	-	P	Equiaxial, t, d	C+(F+A)
	VNSP153D	1,08	α	-	-	P	Equiaxial, t, d	C+(F+A)
	VNSP154D	1,58	α	-	-	P	Equiaxial, t, d	C+(F+A)
	VNSP155D	0,79	α	-	-	P	Equiaxial, t, d	C+(F+A)
	VNSP165D	1,42	α	-	-	P	Equiaxial, t, d	C+(F+A)
	VNSP178D	<0,07	α	-	-	P (eutectic)	Equiaxial, t, d	C+(F+A)
	VNSP268D	<0,07	α	-	-	P	Equiaxial, t	C+(F+A)
E – Blades, Arrowheads	VNSP180E	5,57	α, As-rich	-	P	P	Equiaxial, s, t, d,	C+(F+A)+FF↓
	VNSP181E	2,22	α	-	-	P	Equiaxial, t, d, sb	C+(F+A)+FF
	VNSP182E	5,66	α	-	-	-	Equiaxial, t, d	C+(F+A)
	VNSP183E	3,89	α, As-rich	-	P	-	Equiaxial, s, t, d, sb	C+(F+A)+FF
F - Saws	VNSP185F	0,09	α	-	-	P (eutectic)	Equiaxial, t, d	C+(F+A)
	VNSP186F	<0,07	α	-	-	P (eutectic)	Equiaxial, t, d	C+(F+A)
	VNSP187F	<0,07	α	-	-	P (eutectic)	Equiaxial, t, d	C+(F+A)
G - Daggers	VNSP177G	<0,07	α	-	-	P (eutectic)	Equiaxial, t, d	C+(F+A)
	VNSP188G	1,79	α, As-rich	-	P	P	Equiaxial, t, d	C+(F+A)
	VNSP189G	4,53	α, As-rich	-	P	P	Equiaxial, s, t, d, sb	C+(F+A)+FF
H - Socket	VNSP190H	1,57	α	-	-	P	Equiaxial, t, d	C+(F+A)
I – Indet.	VNSP025I	3,37	α, As-rich	-	P	P	Equiaxial, s, t, d, sb	C+(F+A)+FF
	VNSP184I	3,85	α, As-rich	-	P	P	Equiaxial, s, t, d	C+(F+A)
	VNSP191I	5,49	α, As-rich	-	P	P	Equiaxial, s, t, d,	C+(F+A)+FF↓
	VNSP192I	3,13	α	-	-	P	Equiaxial, t, d	C+(F+A)
	VNSP193I	2,32	α, As-rich	-	P	P	Equiaxial, s, t	C+(F+A)
	VNSP194I	0,51	α	-	-	P	Equiaxial, t?, d?	C+F?
	VNSP196I	0,86	α	-	-	P	Dendritic?	C

Appendix VII – Vickers MicroHardness measurements of VNSP artefacts

Table VII.1. Vickers MicroHardness measurements (HV0.2).

Applied in three different locations of the artefact (when justified) and microstrutural characterization (C – Casting; A – Annealing; F – Forging; FF – Final Forging); * Sample refers to the same artefact cut in two directions - Longitudinal and Transversal; ** Profile of measurements made separately.

Typologies	Artefacts	As (%)	HV0.2 center	HV0.2 blade	HV0.2 fracture	Operatial Sequence
A - Awls	VNSP001A	4,36	80	-	-	C+(F+A)+FF
	VNSP021A	0,90	40	-	-	C+(F+A)
	VNSP023A	0,96	68	-	-	C+(F+A)
	VNSP029A	3,19	59	-	-	C+(F+A)
	VNSP031A	1,43	106	-	-	C+(F+A)
	VNSP038A	1,56	81	-	-	C+(F+A)
	VNSP040A	3,39	60	-	-	C+(F+A)+FF↓
	VNSP047A	<0,07	63	-	-	C+(F+A)
	VNSP049A	5,59	65	-	-	C+(F+A)
	VNSP097A	6,04	86	-	-	C+(F+A)+FF↓
B - Wires	VNSP123B	0,21	84	-	-	C+(F+A)
	VNSP124B	0,19	91	-	-	C+(F+A)
C - Chisels	VNSP132C	4,92	53	-	-	C+(F+A)
	VNSP133C	0,27	36	-	-	C+(F+A)
	VNSP134C	<0,07	81	-	-	C+(F+A)
	VNSP135C	1,53	42	-	-	C+(F+A)
	VNSP136C	<0,07	94	-	-	C+(F+A)
	VNSP137C	<0,07	85	-	-	C+(F+A)+FF↓
	VNSP138C	1,08	44	-	-	C+(F+A)
	VNSP139C	1,71	91	115	90	C+(F+A)
	VNSP140C	3,43	80	105	90	C+(F+A)+FF↓
	VNSP262C**	<0,07	-	-	-	C+(F+A)
	VNSP141C	2,61	97	123	98	C+(F+A)+FF↓
D - Axes	VNSP144D	<0,07	44	66	47	C+(F+A)
	VNSP145D T*	<0,07	48	50	49	C+(F+A)
	VNSP145D L*	<0,07	53	50	49	C+(F+A)
	VNSP146D	2,04	45	47	45	C+(F+A)
	VNSP147D	1,85	65	57	64	C+(F+A)
	VNSP148D	9,13	95	95	95	C+(F+A)
	VNSP150D	0,24	45	50	49	C+(F+A)
	VNSP153D	1,08	64	64	65	C+(F+A)
	VNSP154D	1,58	47	46	45	C+(F+A)
	VNSP155D	0,79	42	45	45	C+(F+A)
	VNSP165D	1,42	42	47	46	C+(F+A)
	VNSP178D	<0,07	75	-	-	C+(F+A)
	VNSP268D	<0,07	41	50	45	C+(F+A)
E – Blades,	VNSP180E	5,57	63	63	75	C+(F+A)+FF↓
Arrowheads	VNSP181E	2,22	119	119	120	C+(F+A)+FF
	VNSP182E	5,66	90	96	75	C+(F+A)
	VNSP183E	3,89	54	55	53	C+(F+A)+FF
F - Saws	VNSP185F	0,09	53	42	46	C+(F+A)
	VNSP186F	<0,07	73	73	73	C+(F+A)
G - Daggers	VNSP177G	<0,07	43	44	46	C+(F+A)
	VNSP188G	1,79	77	80	78	C+(F+A)
	VNSP189G	4,53	155	204	119	C+(F+A)+FF
H - Socket	VNSP190H	1,57	48	-	-	C+(F+A)
I - Indeterminate	VNSP025I	3,37	157	-	-	C+(F+A)+FF
	VNSP184I	3,85	51	51	51	C+(F+A)
	VNSP191I	5,49	61	-	-	C+(F+A)+FF↓
	VNSP192I	3,13	48	-	-	C+(F+A)
	VNSP193I	2,32	50	44	-	C+(F+A)
	VNSP194I	0,51	90	-	-	C+F?
	VNSP196I	0,86	-	-	-	C

Table VII.2. Vickers MicroHardness (HV0.2) measurements of Chisel VNSP262C. Applied in two directions.

VNSP262C – Vickers microhardness profile		
Points	**Transversal (T)**	**Longitudinal (L)**
1	116	93
2	103	98
3	99	97
4	99	93
5	91	101
6	91	93
7	90	90
8	86	86
9	86	84
10	88	88
11	89	93
12	89	94
13	89	85
14	91	89
15	103	91
16		87
17		82
18		88
19		82
20		89
21		88
22		88
23		85
24		90
25		80
26		90
27		89
28		88
29		82
30		81
31		83
32		80
33		77
34		78
35		74
37		80
38		83
39		80
40		79
41		83
42		78
43		86
44		84
45		92